Mixing belOw Tropical Instability waVEs 2024 (MOTIVE) Cruise Report

Nov 5-Dec 8, 2024, *RV Sikuliaq*

Caitlin Whalen (Chief Scientist) Gunnar Voet (Co-Chief Scientist)
Waen Anutaliya Zoe Caspar-Cohen, Nicole Couto Ellen Davenport
Andrew Davies Anna Deppenmeier Caique Dias Luko Helen Dufel
Sara Goheen Kayleigh Jones Jofia Joseph Spencer Kawamoto
Katie Kohlman, Arnaud Le Boyer Alex Negrila Michal Shaham

Updated: January 8, 2025

Motivation

The equatorial Pacific is home to a complex current system and the El Ninõ Southern Oscillation (ENSO), which has profound implications for ecosystems and human communities that surround the Pacific basin. Mixing processes across isopycnals are thought to be important for governing the vertical transport of heat in the region, thereby playing a key role in modulating the ENSO cycle. However, the full range of mechanisms responsible for mixing are currently unknown. Recent modeling studies and observations suggest that Tropical Instability Waves (TIWs), which rim the equatorial cold tongue during La Ninã and neutral ENSO states, may set near equatorial mixing rates by altering the generation, propagation and/or breaking of internal waves. To investigate this, the observations were designed to address the questions: What processes govern the observed modulation of internal waves, and possibly turbulent mixing, by TIWs in the equatorial Pacific? and, Do these processes play a large enough role in heat regulation to be significant in ENSO dynamics?

To understand how TIWs modulate mixing in the equatorial Pacific, we made high temporal and spatial resolution measurements of velocity, density, and microstructure turbulence (shear and temperature) using ship-mounted acoustics, ship-based profiling systems, moorings, and autonomous drifting platforms including:

1. The deployment of three moorings between 0.5° and 3° north of the 140°W Tropical Atmosphere Ocean (TAO) mooring at the equator to target the seasonal cycle in TIW-modulation of internal waves and turbulent mixing.

2. Shipboard measurements using the Multiscale Ocean Dynamics (MOD) FastCTD and Epsifish systems, targeting westward propagating TIW fronts to closely examine the generation and/or modulation of the internal wave field and associated turbulent mixing processes below the equatorial undercurrent (EUC) with the passage of TIWs.

3. Measurements using the shipboard ADCPs (os38, os75, and wh300), EK80, WAMOS, and ship-based thermosalinograph.
4. Two deployments of an array of freely drifting WireWalkers measuring the upper 750 m of the ocean.
5. A Seaglider deployment with the second WireWalker array deployment.
6. The deployment of three EM-Apex and two BGC-Argo floats.
7. A CPIES array circling Mooring C.
8. Full-depth CTD casts at each of the mooring sites.
9. Two Saildrones followed the 2nd WireWalker array

Timeline

The overall cruise timeline is detailed below where dates/times are in UTC.

Nov 5 The Sikuliaq departs Honolulu

Nov 6-9 FastCTD/Epsi Tests, 3 CTD calibration casts

Nov 11 EM-Apex float deployment

Nov 12 CTD cast at Mooring C cite with BGC water sampling and 2nd EM-Apex float deployment

Nov 12-13 CPIES deployment

Nov 13 Mooring C deployment, BGC Argo float deployment

Nov 14 Deployment of Northern WireWalker array

Nov 14-17 FastCTD/Epsi repeat section at 2.3N

Nov 19 Recovery of Northern WireWalker Array

Nov 19 Full depth CTD cast at Mooring B site

Nov 19 Mooring B deployment

Nov 20 Deployment of Southern WireWalker array, Seaglider deployment

Nov 20 1st occupation of southern FCTD/Espi repeat section at 0.73N

Nov 21 Full-depth CTD cast near Mooring A site with BGC water sampling

Nov 21-22 Mooring A deployment, BGC Argo float deployment

Nov 22-25 Continue occupying the southern FCTD/Espi repeat section at 0.73N

Nov 25 Short meridional FastCTD survey

Nov 25-28 Long zonal FastCTD survey

Nov 28 Short meridional FastCTD survey near WireWalkers and Saildrones

Nov 28 Southern Wirewalker array recovery

Nov 29-Dec 1 Big meridional FastCTD survey

Dec 2 Deploy 3rd EM-Apex float

Dec 8 The Sikuliaq returns to Honolulu

Technical Overview

3.1 Moorings

Gunnar Voet

We deployed three close-to full-depth moorings in a triangle formation between 0.5°N and 3°N near 140°W with 278 km (150 nm) separation distance between the moorings. The general scientific goals for the moorings are measuring shear, stratification, and turbulence over a full seasonal cycle, and to obtain a large-scale vorticity estimate within the triangle. Through an NSF RAPID proposal we added instrumentation on two of the moorings to study turbulence near the bottom. The moorings are equipped with ADCPs, CTDs, temperature sensors, and turbulence-measuring χpods.

Various instruments were calibrated on shipboard CTD casts 1 through 4 (Table 1).

Our general approach for mooring deployments was (a) to obtain multibeam observations over previously chosen sites based on Smith & Sandwell bathymetry to obtain a good bottom depth estimate and to confirm relative flatness of the bottom, (b) to carry out a shipboard CTD cast to within 10 m from the bottom to confirm multibeam measurements, (c) to re-terminate mooring line if needed to adjust mooring length to updated bottom depth estimate, (d) to commence with mooring deployment, and (e) to carry out a trilateration survey if deemed necessary.

For all three moorings we set up to have between 5 and 6 hours for deployment at a towing speed of about 1 knot through the water. We overshot planned deployment sites by 400m to account for anchor fallback of about 10%.

For deck operations we used a Hawboldt mooring winch with pre-spooled mooring wire and a small winch mounted on the A-frame. We set up two cleats and used one hook- and one slip-line for stopping off between segments. The A-frame winch was used to both deploy the bigger syntactic foam floats and to hang the MOD 508 traveling block. Anchors were put inside the A-frame near the transom prior to and ready for deployment which proved to be quite comfortable. We had excellent support from the ship's crew during deck operations.

CTD Cast	Maximum Depth	Instruments
1	1200 m	SBE56, 1700 m-rated RBR Solo, 3500 m-rated SBE37
3	500 m	SBE39
4	>4000 m	10 km-rated RBR Solo, 7 km-rated SBE37

Table 1: Mooring instrument calibrations on shipboard CTD casts.

MOTIVE C was deployed Nov 13, 2024. Based on multibeam and CTD measurements we had to shorten the mooring by about 16 m. Operations went smoothly without any notable events. We skipped the trilateration survey and may do one on recovery.

MOTIVE B was deployed Nov 19, 204. We added two extra line shots we had on hand (100 m and 44 m) to account for larger bottom depth than expected. Operations again went very smoothly. We were ready for the anchor drop quite a bit ahead of time and decided to drop the anchor a bit earlier northeast of the planned site as the bottom was quite flat and exact positioning did not matter due to the large size of the mooring triangle. We dropped the anchor at 20:55 UTC. Based on our approach route, drop location, and anchor fallback, our best estimate for the mooring site is 137° 49.553' W, 1° 45.907' N. Multibeam depth at this site was 4327 m. We did not obtain a location estimate via trilateration to save time.

MOTIVE A was deployed Nov 21, 2024. Bottom depth compared well with Smith & Sandwell and we did not have to adjust mooring length. For setup, we did not account for much of the mooring catenary hanging into the relatively strong EUC at this site. Winds were relatively strong and not well aligned with the EUC. At some point during the deployment, we started having a sharp angle towards starboard with the mooring almost taking us over. The ship was able to reset at a different approach angle. We still were not able to make it to the original drop site and landed in about 40 m deeper waters. The anchor was dropped at 04:01:39 UTC. We did a trilateration survey at this site due to the different drop location. Trilateration points were chosen a bit too close to the location such that one of the survey points appears to have been almost directly over the site. We had to use the over-the-side transducer as the ship transducer didn't seem to work well. Location is 0° 31.299' N, 139° 59.712' W at 4389 m multibeam depth.

3.2 WireWalkers

Caique Dias Luko

Wirewalkers are vertical-profiling platforms powered by ocean waves. Several sensors can be easily integrated to wirewalkers, which allows concurrent, rapid and high vertical resolution sampling of different key ocean variables. The Wirewalker system is composed by a buoy, a wire, the wirewalker platform, and bottom weights. Wirewalkers can be deployed as anchored moorings, or as drifting moorings. During the cruise, we deployed three drifting wirewalker systems twice. Each wirewalker had a different configuration, including different sensors and lengths of wire:

- Wirewalker systems 1 and 2: These Wirewalkers spanned 750 m and were equipped with a CTD (RBR Concerto), a 4 beam ADCP (Nortek Signature 1000), an Epsi-minnow system (MOD), a Dissolved Oxygen Sensor (RBR coda^3 T.ODO), and a RBR Tridente with fluorescence and backscatter channels. Wirewalker 1 was also equipped with a RBR solo^3 PAR (Photosynthetically Active Radiation) and with a surface shortwave radiation sensor attached to the buoy (DL4-I07 Pyronometer).

- Wirewalker system 3: This Wirewalker system was composed of two wirewalkers. The first one spanning the upper 100 m and the second one spanning from 100 m to 750 m. The upper wirewalker was named WW4 and was equipped with a CTD (RBR concerto), and a 5 beam ADCP (Nortek Signature 1000). The lower wirewalker was named WW3 and was equipped with a CTD (RBR Concerto), a 4 beam ADCP (Nortek Signature 1000), an Epsi-minnow

	Depl.	Range	Time Start (UTC)	Time End (UTC)	Avg. Round Trip Time	Number of Profiles
WW1	1	0-750 m	2024-11-14 10:29	2024-11-18 22:50	55 minutes	119
WW2	1	0-750 m	2024-11-14 12:41	2024-11-18 21:00	55 minutes	114
WW3	1	100-750 m	2024-11-14 13:04	2024-11-18 19:29	44 minutes	138
WW4	1	0-100 m	2024-11-14 12:58	2024-11-18 19:29	11 minutes	531
WW1	2	0-750 m	2024-11-20 10:26	2024-11-28 23:49	58 minutes	211
WW2	2	0-750 m	2024-11-20 11:55	2024-11-28 19:47	1 hour	196
WW3	2	100-750 m	2024-11-20 12:23	2024-11-28 21:54	53 minutes	229
WW4	2	0-100 m	2024-11-20 13:35	2024-11-28 21:34	10 minutes	1116

Table 2: Wirewalker deployment information and profiling performance.

system (MOD), a Dissolved Oxygen Sensor (RBR coda^3 T.ODO), and a RBR Tridente with fluorescence and backscatter channels.

The ADCP, RBR Concerto, Tridente and ODO sensors were set to sample on continuous mode at 8Hz sampling rate, while the PAR sensor was set to sample every 2 s. The ADCP ran simultaneously on Burst and Burst High-Resolution mode, with configurations supporting velocity measurements both on a 30 m range with 1 m resolution, as well as a 3 m range with 0.12 m. The High-Resolution measurements will be used in the future to estimate dissipation of turbulent kinetic energy (ε) through structure functions.

Prior to the actual deployments, the ADCPs were compass calibrated at the dock using the Signature Deployment Nortek software. The RBRcoda^3 T.ODO was calibrated pre- and post-deployment by immersing the sensor for an hour in saturated and oxygen-depleted solutions. The saturated solution is a 800 mL water solution aerated with an aquarium pump, while the oxygen-depleted solution is achieved by adding 30 g of Sodium Sulfite to 800 mL of water. To calibrate the RBR Concerto and Tridente we attached them to the ship's Rosette and performed a CTD cast at 12°37.8′N and 149°32.9′W. The Concerto measurements will be calibrated against the ship's CTD, while the Chlorophyll measurements will be calibrated against chlorophyll samples collected during the cast. Water samples (and duplicates) were taken at 6 depths (3 below the chlorophyll maximum, 1 at the chlorophyll maximum, and 2 shallower than the chlorophyll maximum). Samples were drained from Niskine bottles and stored on 250 ml calibrated bottles after rinsing them three times. The samples were then filtered using 25 mm Whatman GF/F paper filters. The paper filters were then folded and stored on paper foil before being frozen. Finally, the samples were sent back to the ODF lab at Scripps to be analyzed.

The first wirewalker deployment lasted for about four days (Figure 1). The wirewalkers were deployed at about 2.3°N 138.2°W as a triangle west of a TIW leading edge front. During the deployment, the wirewalkers moved north from warmer waters towards the TIW cold cusp edge. As they approached the front, the strong surface convergence deformed their triangle formation into a line. After four days, we recovered the Wirewalkers and re-deployed them south at about 0.7°N 139.1°W. The second deployment lasted for about 8.5 days (Figure 2). The Wirewalkers were deployed slightly east of a leading edge TIW front, and were recovered after crossing a big portion of the TIW cold cusp. In total, the wirewalkers performed 2654 profiles, providing high vertical resolution data (0.25m for T, S and BGC variables and 1 m for currents) from the surface down to 750 m with 1 hour resolution for the deep ranging systems, and 10 minutes resolution for

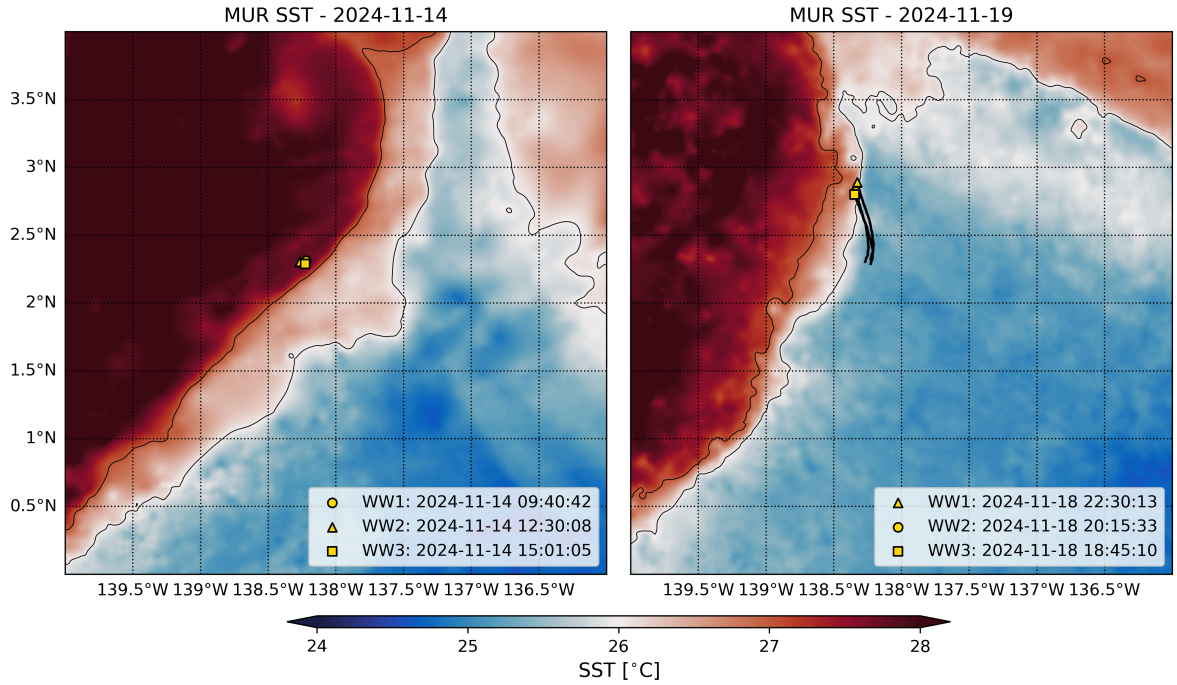

Figure 1: Wirewalker Trajectories and Sea Surface Temperature (MUR) maps during the: (left) start of the first deployment, and (right) end of the first deployment.

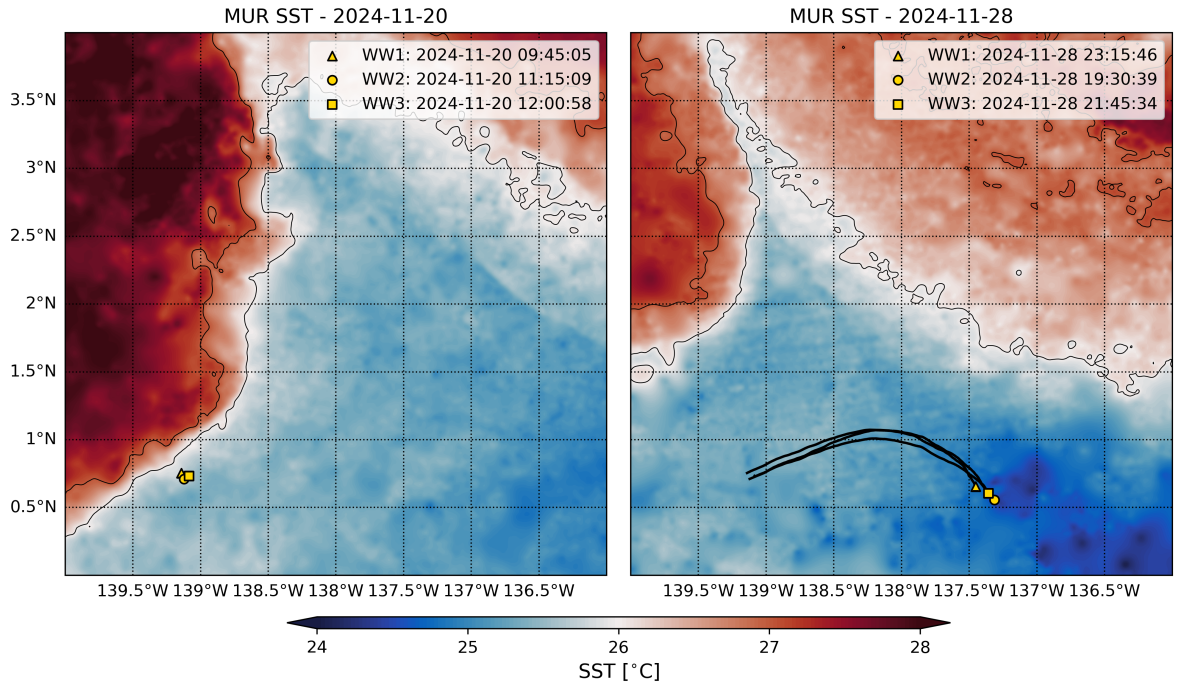

Figure 2: Wirewalker Trajectories and Sea Surface Temperature (MUR) maps during the: (left) start of the second deployment, and (right) end of the second deployment.

the 100 m range system (See Table 2 for more details). Turbulent measurements were also obtained with the Epsilometer (Figs 3 and 4) and are going to be used to compute heat, momentum and biogeochemical fluxes. This high-resolution wirewalker dataset allowed us to observe different phenomena such as shear-layers at depth, Deep Cycle Turbulence, and the impacts of mixing and fronts on biogeochemistry. These observations are further described in Section 4.

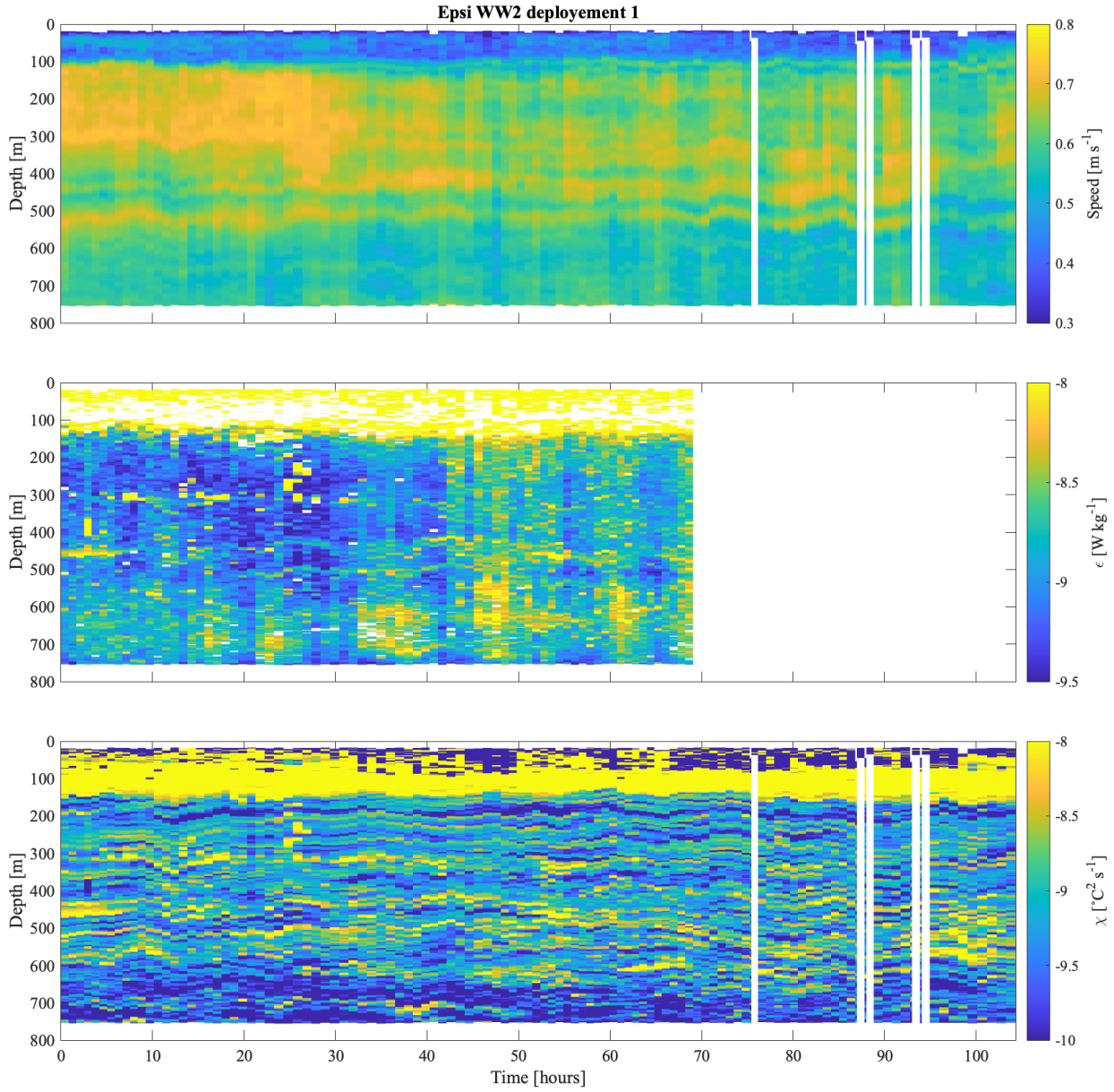

Figure 3: Epsilometer data from the first deployment (Upfront). Top panel: Wirewalker ascent Velocities. Middle panel ε. Lower panel χ. Post-Cruise Processing, the final product will need the application of the QC flag.

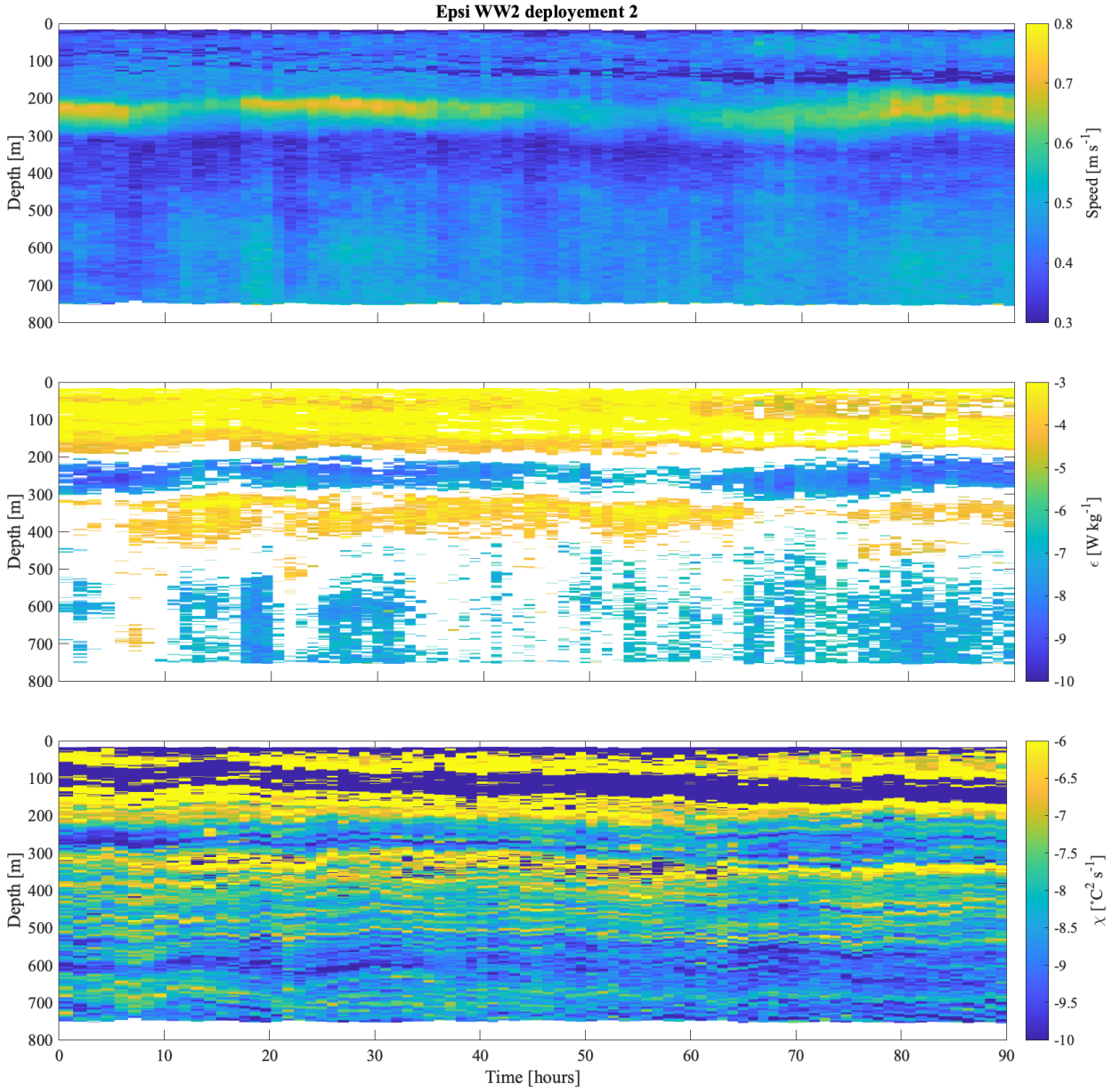

Figure 4: Epsilometer data from the second deployment (Down front). Top panel: Wirewalker ascent Velocities. Middle panel ε. Lower panel χ. Post-Cruise Processing, the final product will need the application of the QC flag.

3.3 FastCTD / Epsifish

Nicole Couto and Arnaud Le Boyer

We collected 13 zonal and meridional sections measuring hydrography and turbulence parameters using the FastCTD winch system, built by the Multiscale Ocean Dynamics group (MOD) at SIO, and two different profilers. The FastCTD carried a Seabird SBE49 CTD, an RBRtridente

Depl.	Instrument	Start Date	No. of Casts	Notes
d1-6	FCTD and Epsilometer	11/5		Engineering tests (not shown in Figure). No science goals
d7	FCTD	11/14	163	Eastward cross-front section at 2.25 N
d8	Epsilometer	11/15	33	Westward cross-front section at 2.25 N
d9	FCTD	11/16	135	Eastward cross-front section at 2.25 N
d10	Epsilometer	11/17	54	Westward cross-front section at 2.25 N
d11	FCTD	11/20	96	Westward survey from the 2nd Wirewalker array deployment location towards Mooring A
d12	FCTD	11/22	4	Uncoiling the FCTD cable. No science goals.
d13	Epsilometer	11/22	38	Eastward section at 0.7 N
d14	FCTD	11/22	84	Westward section at 0.7 N
d15	Epsilometer	11/24	26	Eastward section at 0.7 N
d16	FCTD	11/24	32	Westward section at 0.7 N
d17	FCTD	11/24	30	Northward section
d18	FCTD	11/25	287	Eastward section aiming to cross the leading and trailing ends of the instability wave front
d19	FCTD	11/27	37	Southward section in the vicinity of the Saildrones and Wirewalkers
d20	FCTD	11/29	201	Northward section starting at the Equator

Table 3: FCTD and Epsilometer deployment details.

fluorometer, and a microconductivity probe. The MOD-designed Epsilometer carried a Seabird SBE49 CTD, two shear probes and two FPO7 fast-response temperature probes. Each deployment is briefly described in Table 3.

Deployments d7-d10 and d11-d16 were repeat transects along a single latitude (2.25° N and 0.7° N respectively). On these transects we alternated using the FastCTD and Epsifish depending on the direction we were steaming. We chose the direction for Epsifish profiling based on the direction of the strongest currents; since Epsifish is a freefalling profiler, using it while steaming against a current would lead to excessive line payout with the possibility of running out of cable before achieving the target depth. For the deployments at 2.25° N, where there was a westward surface current, we profiled with Epsifish on the westward transects. For the deployments at 0.7° N, where there was a strong eastward surface current, we profiled with Epsifish on the eastward transects.

The following section plots show a summary of CTD, ADCP and microstructure data from all deployments (Figs. 6-18). The results presented are raw, and using these data will require QC flags for publication. This first section shows several "fake" short profiles due to inefficient profile identification during post-processing. This can be fixed in post-cruise processing. However, the micro-conductivity sensor and its associated χ_T had an issue, and the collected data could not be used. This is fixed for the next transects. As expected in this part of the equatorial ocean and the measured depths, temperature and salinity decrease with depth. A clear signal of the EUC can be seen in velocity, shear, N^2 and χ data between 150-200 m (ex. Fig. 7).

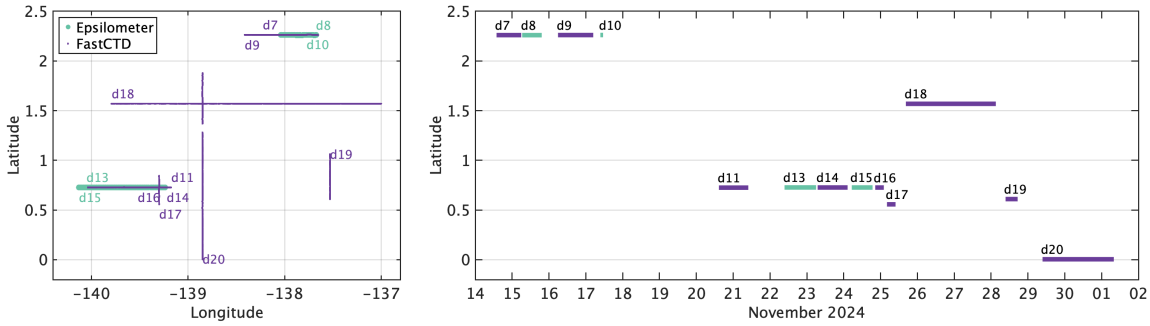

Figure 5: FastCTD and Epsilometer sections collected during the cruise. Left side shows their location on a map and right side shows their timing. For more deployment details, see Table 3

3.4 CPIES

Andrew Davies

The six CPIESs were deployed around one of the moorings as part of a larger effort to deploy Internal Wave Resolving (IWR) Arrays throughout the global ocean as part of the National Ocean Partnership Program (NOPP) Global Internal Wave (GIW) study. The project: "A Distributed Network of Internal Wave Resolving Moored Arrays for Assessing Tide-Resolving Model Fields and Improving Forecasts in the Coastal Ocean" is led by PI A. Waterhouse at SIO and is funded by the Office of Naval Research with a subaward for the CPIES component of the arrays to M. Andres at WHOI. The IWR Arrays combine a high vertical-resolution mooring to resolve the waves' modal structure with an antenna of vertically-integrated measures of variability to resolve the speed and direction of beam propagation.

The CPIESs will provide hourly measures of bottom pressure and temperature, near-bottom currents (50-m above the seabed), and round-trip surface-to-bottom acoustic travel time. The CPIESs will provide spatial context for the variability observed at the mooring and the mooring will provide high vertical resolution measurements to complement the vertically integrated measurement provided by the acoustic travel times.

This "Equatorial Array" is the second deployment of an IWR Array and follows the successful deployment and recovery of the first IWR Array west of California. The third IWR Array will be deployed off the Aleutian Islands in summer 2025.

ID	Lon (W)	Lat (N)	Depth (m)	IES SN	CM SN	Telem/XPND/Beacon	Release
E1	139.6859	2.9998	4205	283	43	65/69/73	27
E2	139.8415	3.2702	4330	292	256	65/69/73	37
E3	140.1583	3.2724	4319	304	244	65/69/73	48
E4	140.3158	3.0000	4313	306	257	67/71/75	50
E5	140.1583	2.7273	4320	331	112	65/69/73	11
E6	139.8432	2.7262	4317	332	115	66/70/74	12

Table 4: CPIES deployment locations and serial numbers

Deck Setup and Deployment Operations. The overhead heavy lift winch mounted on the A-frame was used for all of the deployment operations. The CPIES was mounted in its stand with

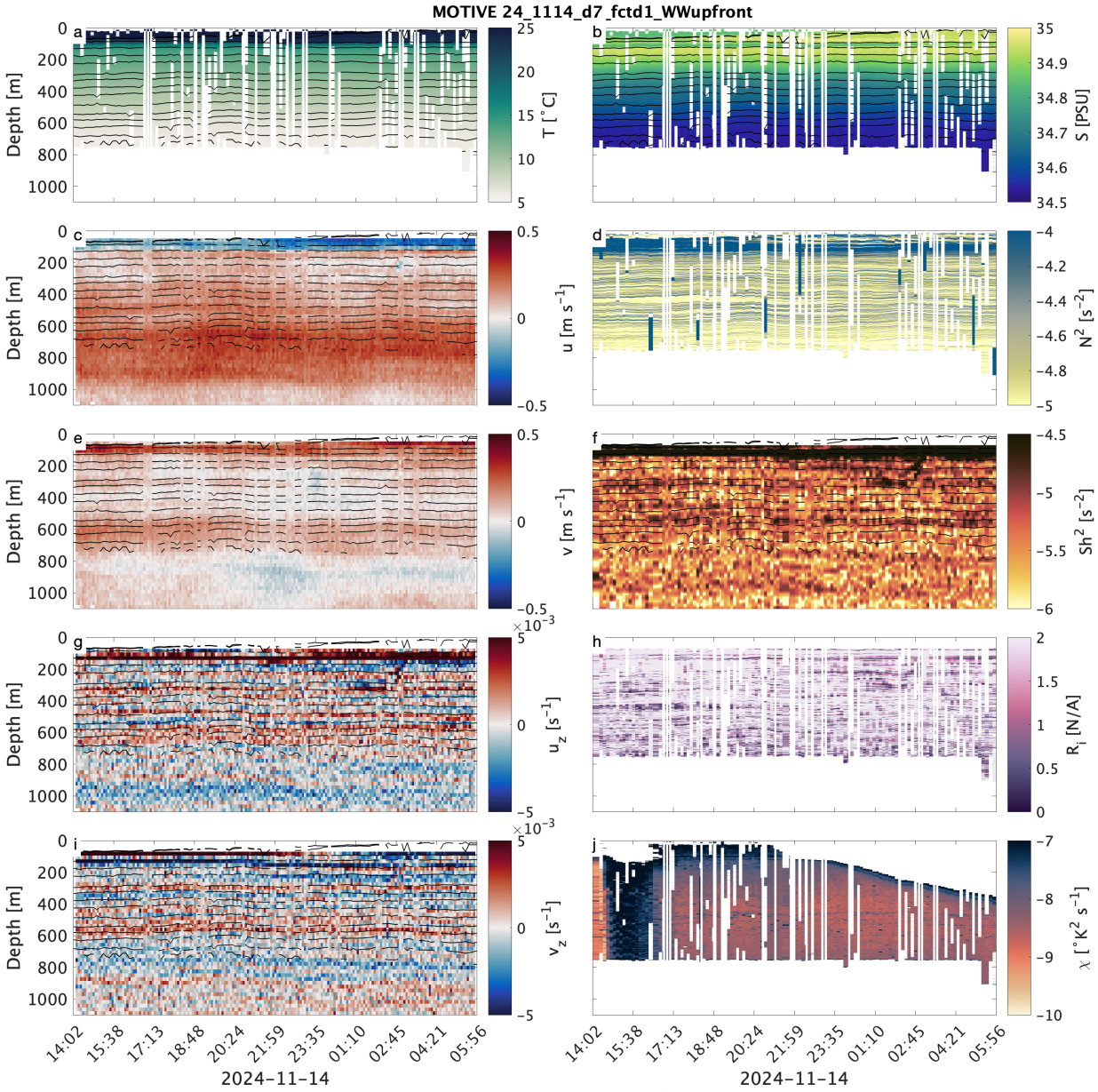

Figure 6: Data collected during section d7 starting at 2.2629 °N 138.2264 °W on 2024-11-14 (UTC) and finishing at 2.2629 °N 138.2264 °W on 2024-11-15 (UTC). a) Temperature. b) Salinity. c) zonal velocity from os38 narrow band. d) N^2. e) Meridional velocity from os38 narrow band. f) Shear squared from os38 narrow band. g) vertical shear from u. h) Richardson number. i) vertical shear from v. j) χ.

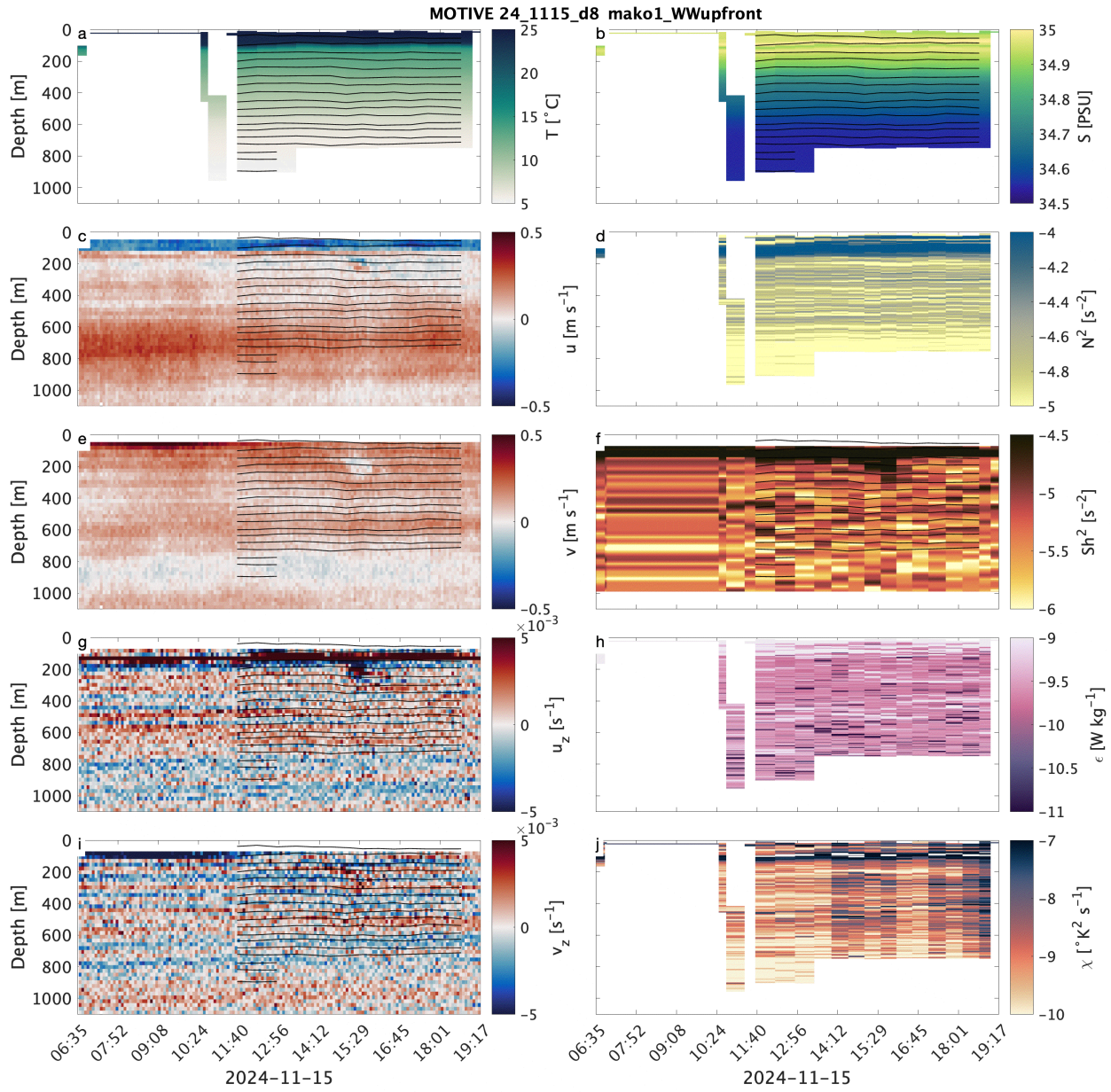

Figure 7: Data collected during section d8 starting at 2.2605 °N 137.6773 °W on 2024-11-15 (UTC) and finishing at 2.2605 °N 137.6773 °W on 2024-11-15 (UTC). a) Temperature. b) Salinity. c) zonal velocity from os38 narrow band. d) N^2. e) Meridional velocity from os38 narrow band. f) Shear squared from os38 narrow band. g) vertical shear from u. h) ε. i) vertical shear from v. j) χ.

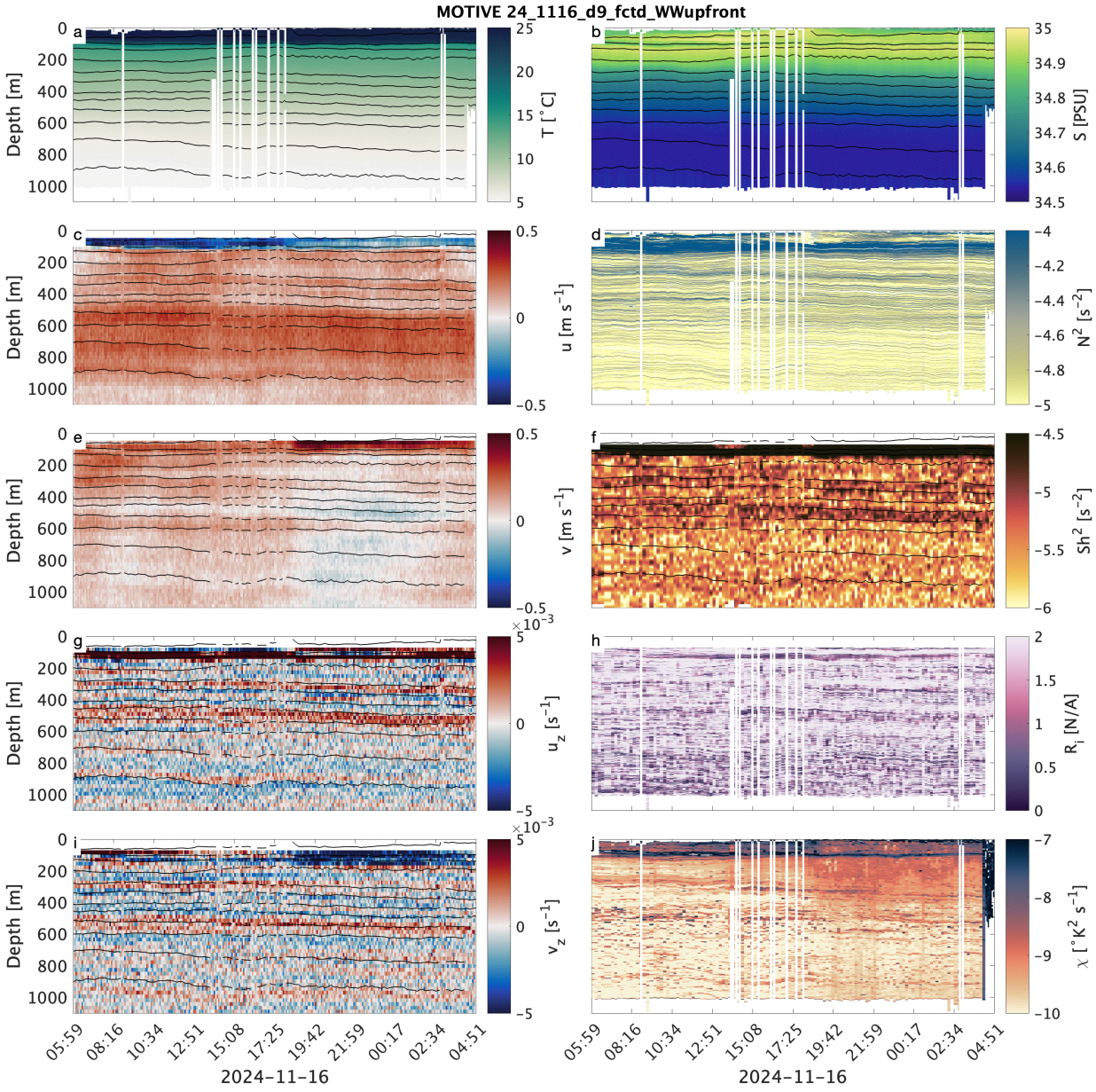

Figure 8: Data collected during section d9 starting at 2.2626 °N 138.4140 °W on 2024-11-16 (UTC) and finishing at 2.2626 °N 138.4140 °W on 2024-11-17 (UTC). a) Temperature. b) Salinity. c) zonal velocity from os38 narrow band. d) N^2. e) Meridional velocity from os38 narrow band. f) Shear squared from os38 narrow band. g) vertical shear from u. h) Richardson number. i) vertical shear from v. j) χ.

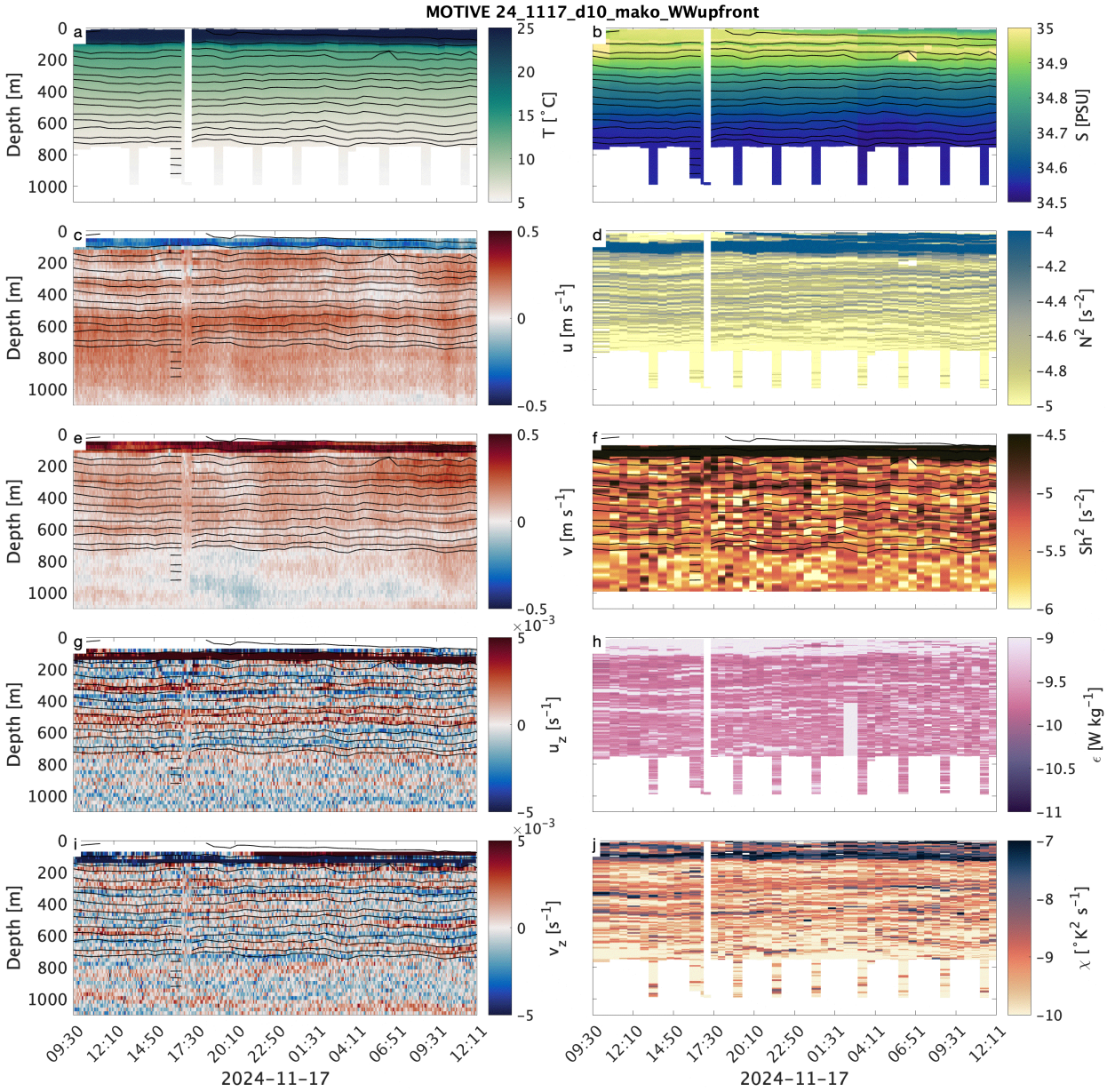

Figure 9: Data collected during section d10 starting at 2.2634 °N 137.7745 °W on 2024-11-17 (UTC) and finishing at 2.2634 °N 137.7745 °W on 2024-11-18 (UTC). a) Temperature. b) Salinity. c) zonal velocity from os38 narrow band. d) N^2. e) Meridional velocity from os38 narrow band. f) Shear squared from os38 narrow band. g) vertical shear from u. h) ε. i) vertical shear from v. j) χ.

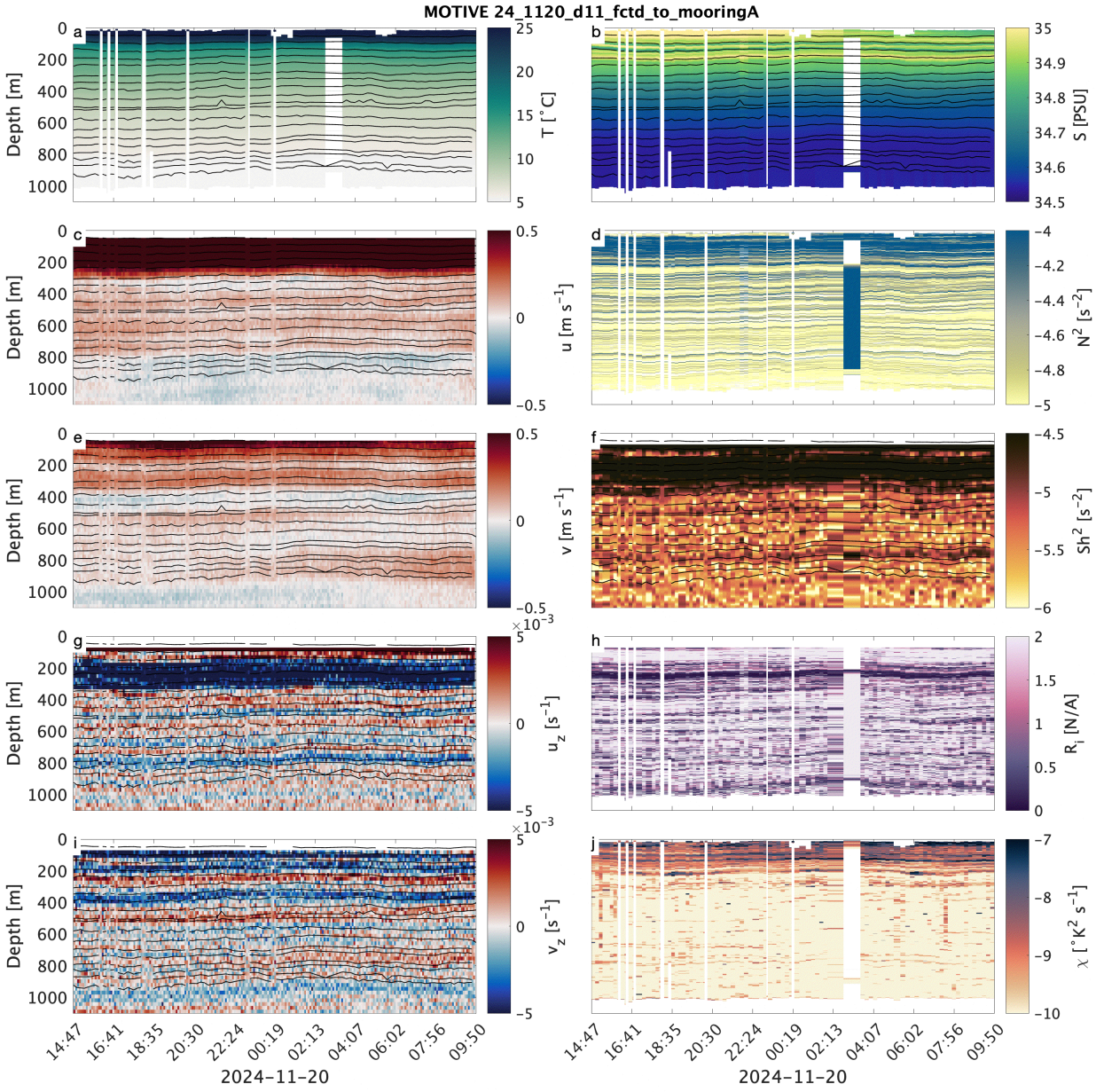

Figure 10: Data collected during section d11 starting at 0.7274 °N 139.1768 °W on 2024-11-20 (UTC) and finishing at 0.7274 °N 139.1768 °W on 2024-11-21 (UTC). a) Temperature. b) Salinity. c) zonal velocity from os38 narrow band. d) N^2. e) Meridional velocity from os38 narrow band. f) Shear squared from os38 narrow band. g) vertical shear from u. h) Richardson number. i) vertical shear from v. j) χ.

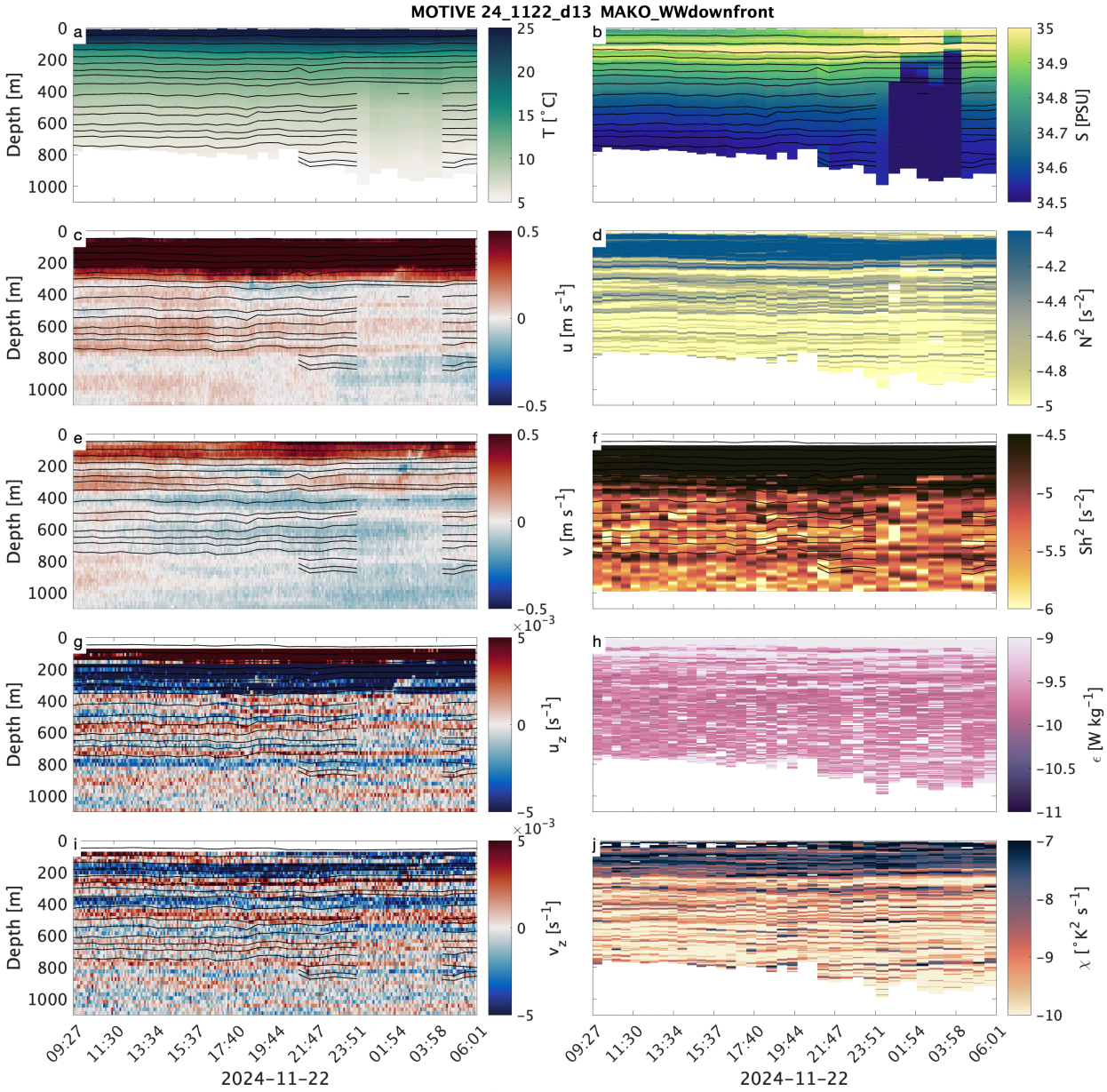

Figure 11: Data collected during section d13 starting at 0.7275 °N 140.0515 °W on 2024-11-22 (UTC) and finishing at 0.7275 °N 140.0515 °W on 2024-11-23 (UTC). a) Temperature. b) Salinity. c) zonal velocity from os38 narrow band. d) N^2. e) Meridional velocity from os38 narrow band. f) Shear squared from os38 narrow band. g) vertical shear from u. h) ε. i) vertical shear from v. j) χ.

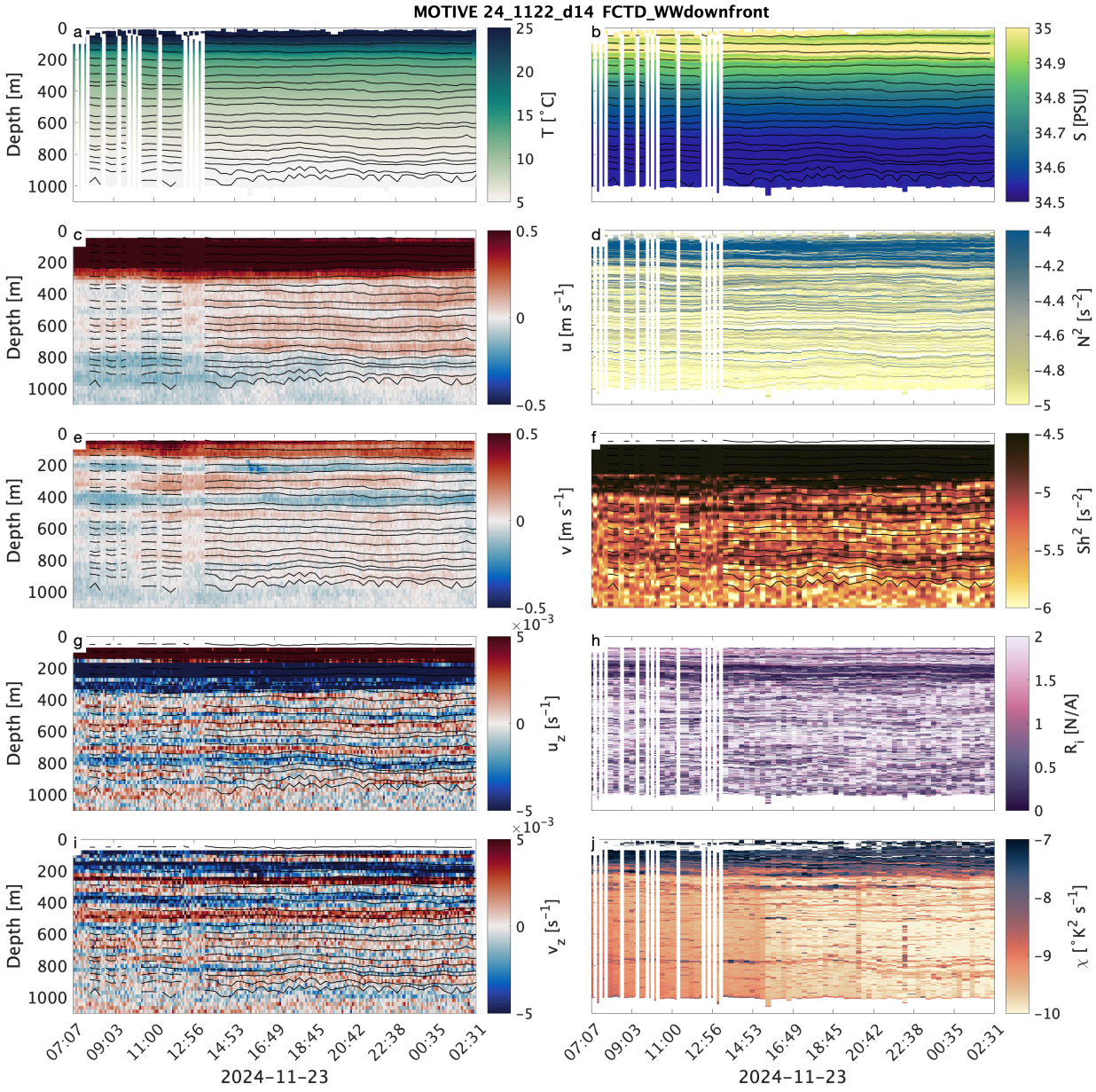

Figure 12: Data collected during section d14 starting at 0.7275 °N 139.2209 °W on 2024-11-23 (UTC) and finishing at 0.7275 °N 139.2209 °W on 2024-11-24 (UTC). a) Temperature. b) Salinity. c) zonal velocity from os38 narrow band. d) N^2. e) Meridional velocity from os38 narrow band. f) Shear squared from os38 narrow band. g) vertical shear from u. h) Richardson number. i) vertical shear from v. j) χ.

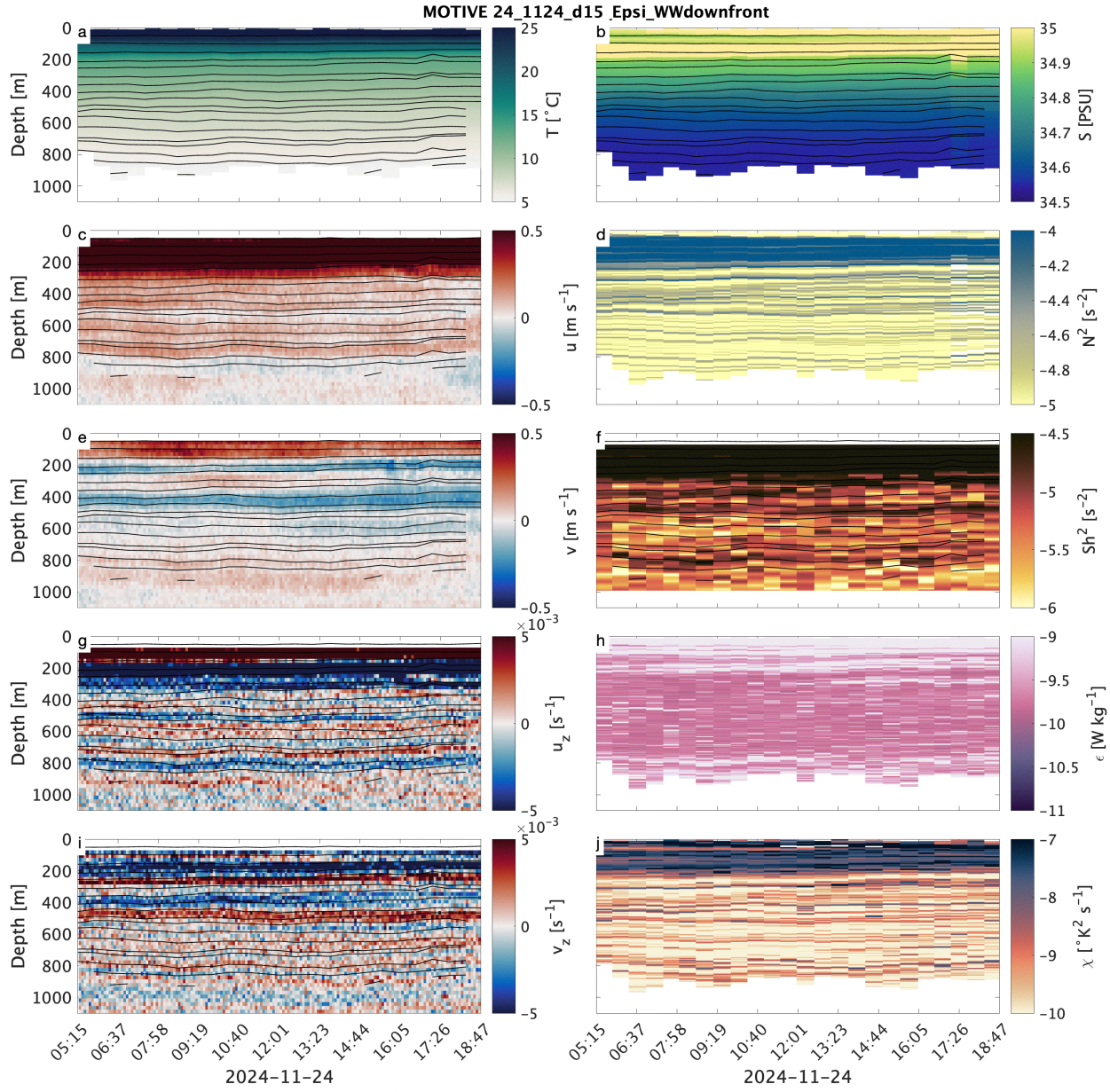

Figure 13: Data collected during section d15 starting at 0.7273 °N 140.1298 °W on 2024-11-24 (UTC) and finishing at 0.7273 °N 140.1298 °W on 2024-11-24 (UTC). a) Temperature. b) Salinity. c) zonal velocity from os38 narrow band. d) N^2. e) Meridional velocity from os38 narrow band. f) Shear squared from os38 narrow band. g) vertical shear from u. h) ε. i) vertical shear from v. j) χ.

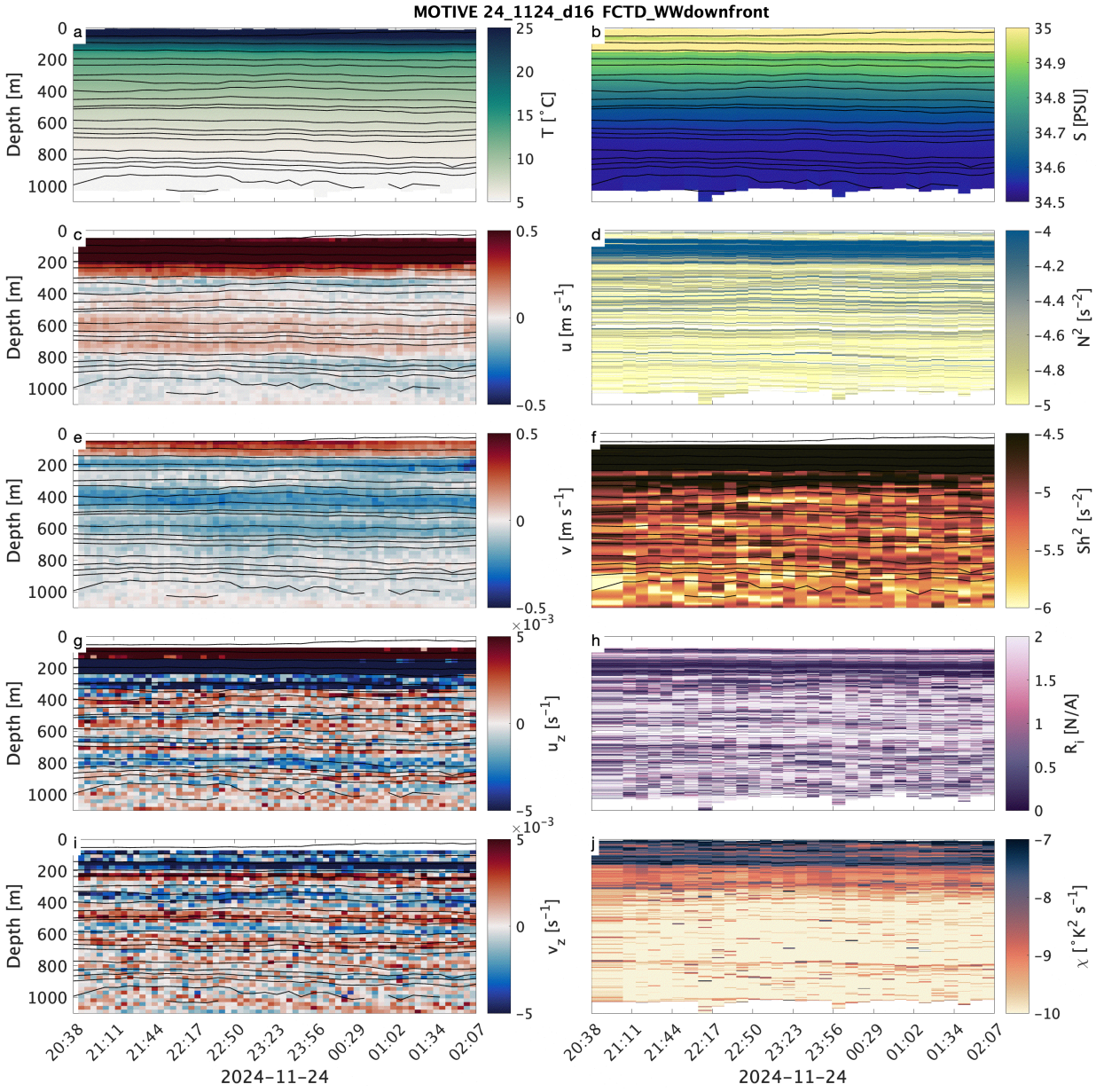

Figure 14: Data collected during section d16 starting at 0.7275 °N 139.5207 °W on 2024-11-24 (UTC) and finishing at 0.7275 °N 139.5207 °W on 2024-11-25 (UTC)). a) Temperature. b) Salinity. c) zonal velocity from os38 narrow band. d) N^2. e) Meridional velocity from os38 narrow band. f) Shear squared from os38 narrow band. g) vertical shear from u. h) Richardson number. i) vertical shear from v. j) χ.

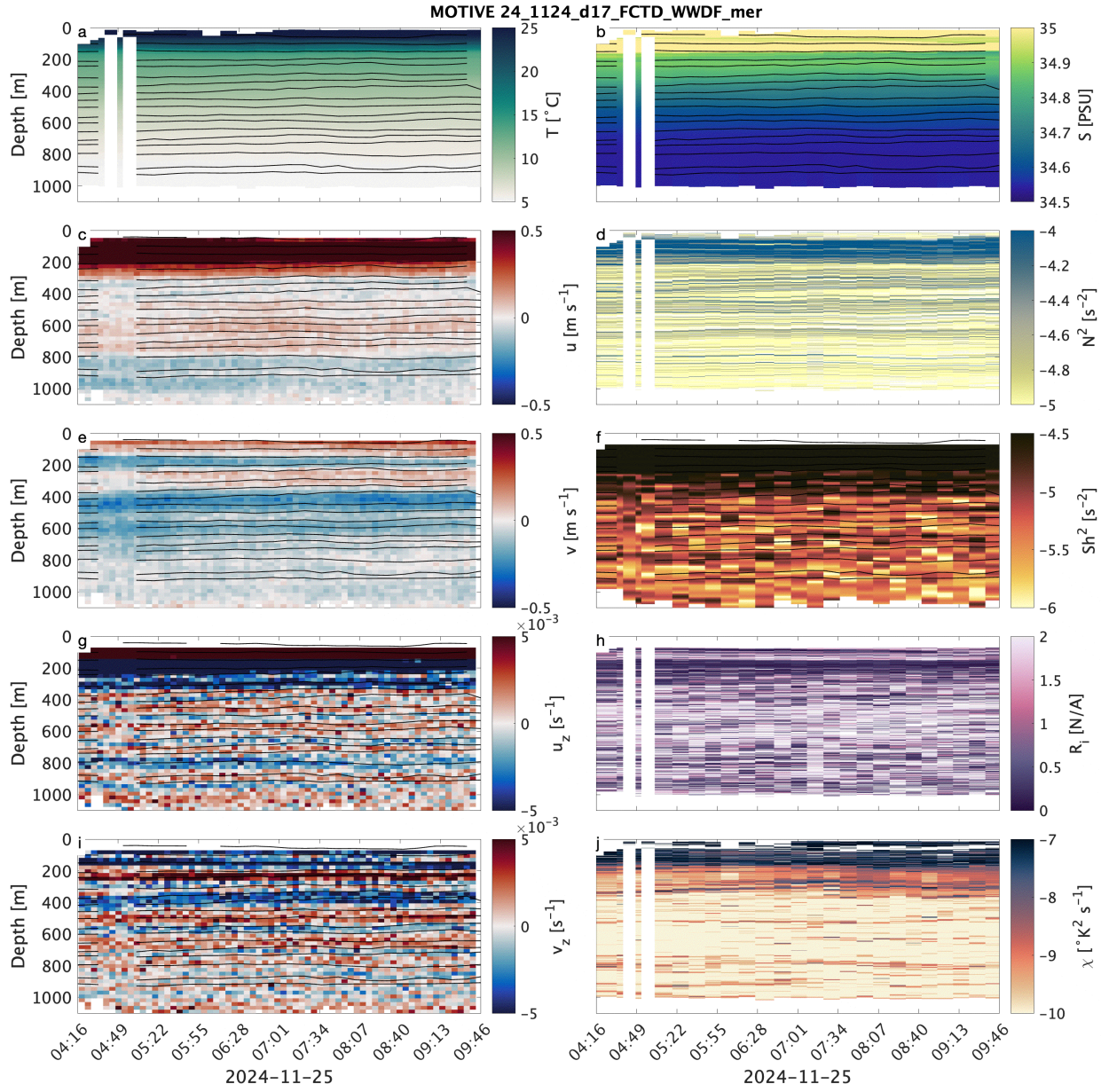

Figure 15: Data collected during section d17 starting at 0.5572 °N 139.2996 °W on 2024-11-25 (UTC) and finishing at 0.5572 °N 139.2996 °W on 2024-11-25 (UTC). a) Temperature. b) Salinity. c) zonal velocity from os38 narrow band. d) N^2. e) Meridional velocity from os38 narrow band. f) Shear squared from os38 narrow band. g) vertical shear from u. h) Richardson number. i) vertical shear from v. j) χ.

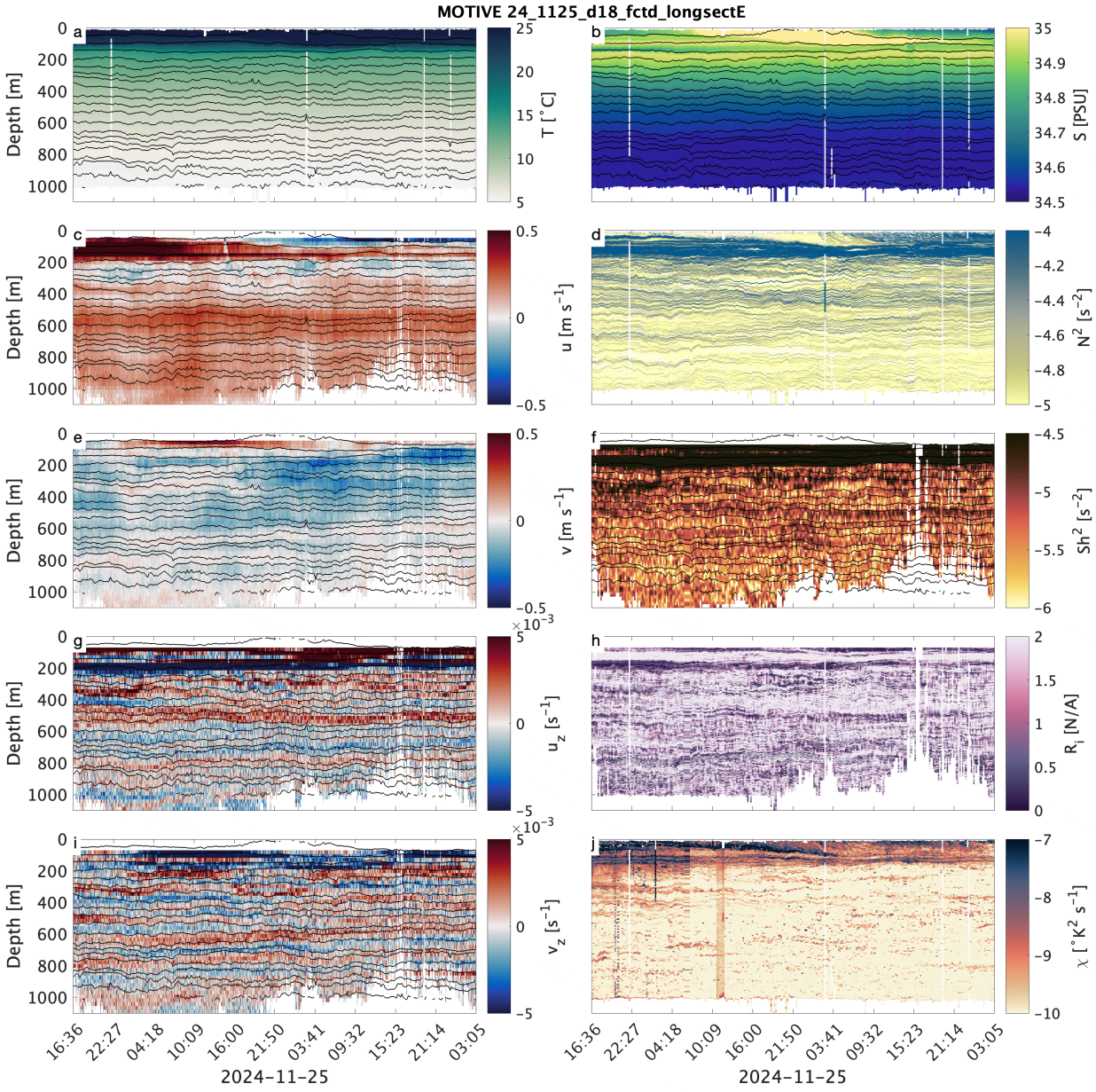

Figure 16: Data collected during section d18 starting at 1.5701 °N 139.7929 °W on 2024-11-25 (UTC) and finishing at 1.5701 °N 139.7929 °W on 2024-11-28 (UTC)) . a) Temperature. b) Salinity. c) zonal velocity from os38 narrow band. d) N^2. e) Meridional velocity from os38 narrow band. f) Shear squared from os38 narrow band. g) vertical shear from u. h) Richardson number. i) vertical shear from v. j) χ.

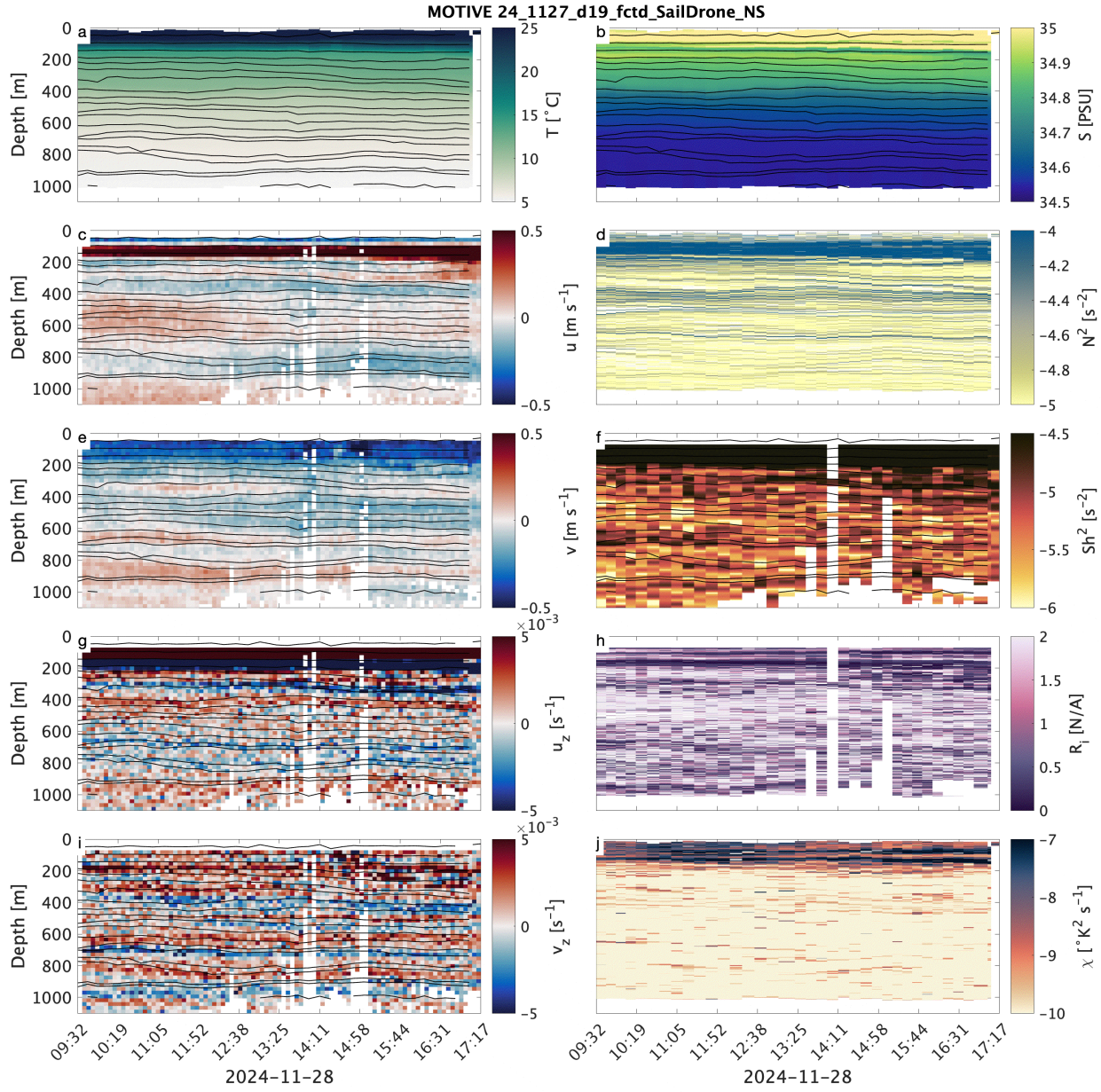

Figure 17: Data collected during section d19 starting at 1.0612 °N 137.5313 °W on 2024-11-28 (UTC) and finishing at 1.0612 °N 137.5313 °W on 2024-11-28 (UTC). a) Temperature. b) Salinity. c) zonal velocity from os38 narrow band. d) N^2. e) Meridional velocity from os38 narrow band. f) Shear squared from os38 narrow band. g) vertical shear from u. h) Richardson number. i) vertical shear from v. j) χ.

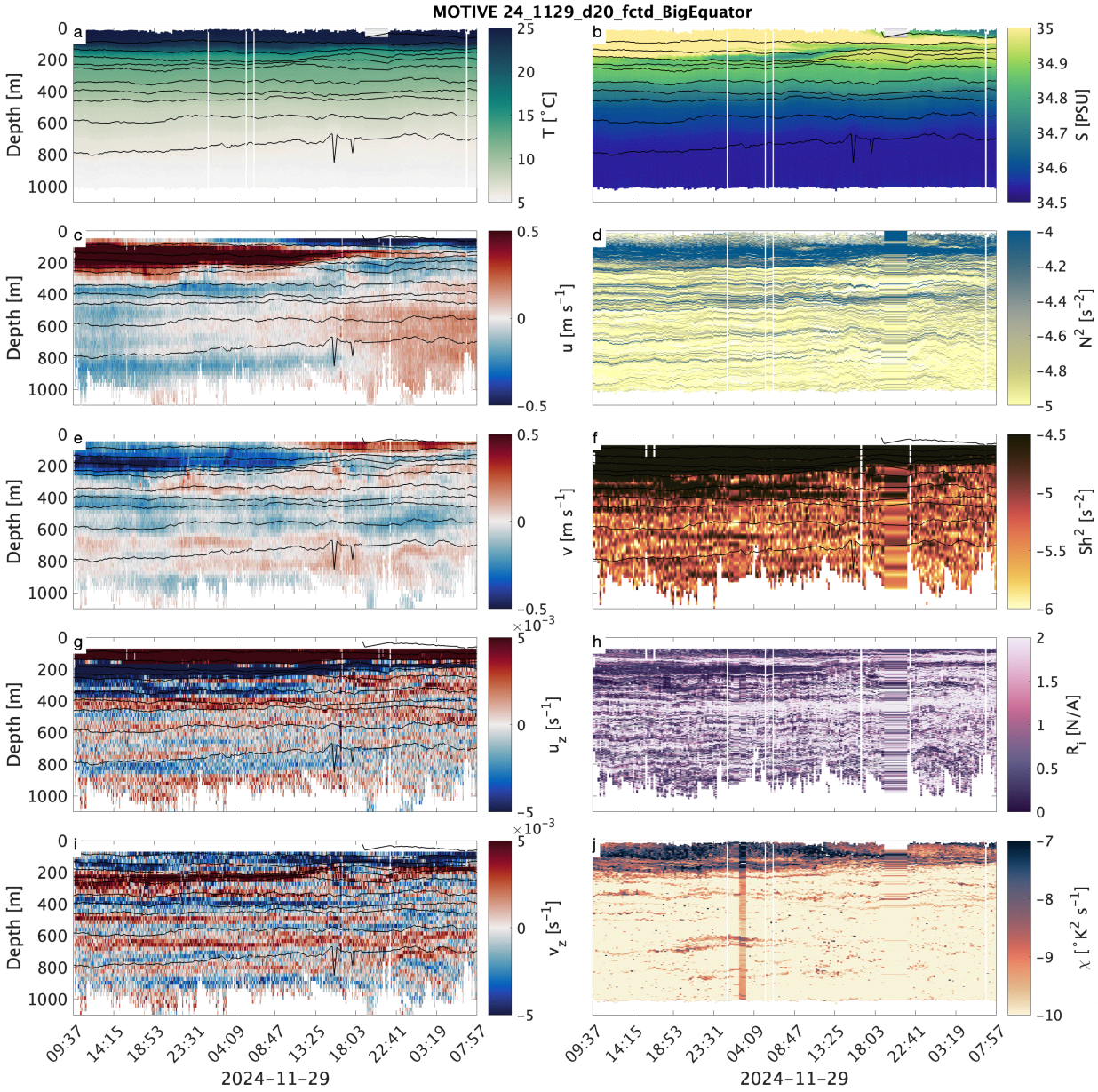

Figure 18: Data collected during section d20 starting at 0.0045 °N 138.8497 °W on 2024-11-29 (UTC) and finishing at 0.0045 °N 138.8497 °W on 2024-12-01 (UTC). a) Temperature. b) Salinity. c) zonal velocity from os38 narrow band. d) N^2. e) Meridional velocity from os38 narrow band. f) Shear squared from os38 narrow band. g) vertical shear from u. h) Richardson number. i) vertical shear from v. j) χ.

(2) 50lb weights attached below, current meter attached and the 50-meter cable was flaked out on deck with a single 17" glass float and recovery line attached above. A quick release was attached to the overhead lifting line to hoist the CPIES for deployment. Prior to deployment, the ship was instructed to move into the seas and toward the drop site at a speed of 1.5 knots. Deployment began when the ship was 80 meters from the site. First, the recovery float and line were streamed into the water followed by the 17" top float, Aanderaa current meter and the 50 meters of cable. When the cable was deployed and taut, the CPIES was hoisted with the winch and A-frame extended outboard. The assembly was pulled away from the ship by the deployed components and lowered to the surface for release. Final CPIES locations are detailed in Table 4.

3.5 BGC Argo Floats

Kayleigh Jones

As part of the NSF-funded Global Ocean Biogeochemical (GO-BGC) Array project, two BGC Argo floats were deployed during the cruise. BGC Argo floats are freely-drifting, autonomous instruments deployed throughout the global ocean. The floats profile to 2000 meters on a ten day cycle, capturing in-situ observations of dissolved oxygen, nitrate, pH, chlorophyll-a, particle backscatter, irradiance, temperature, and salinity. Data is promptly transmitted to remote users through satellite communication.

One BGC Argo float was deployed at the Mooring C location (3°N 140°W) on Nov 13, 2024 and another at the Mooring A location (0.5°N 140°W) on Nov 22, 2024. Deployment locations were chosen to capitalize on the full CTD casts conducted at mooring sites and to fill spatial gaps in the Argo float array. Rosette samples from the surface to 1500 meters were captured and filtered for particulate organic carbon (POC) and high-performance liquid chromatography (HPLC) analysis, to validate float measurements of particle backscatter and chlorophyll-a. Additionally, samples were collected for validation of nutrient (nitrate and nitrite) and pH/alkalinity float observations. At the end of the cruise, all samples were shipped to the Oceanographic Data Facility at the Scripps Institution of Oceanography.

Both floats are operational and successfully transmitting profiles. Data collected by the BGC floats, and the Argo float array at large, gives insight to ecosystem health, productivity, and cycling of nitrogen, oxygen, and carbon. Float observations are also supplemental to the chlorophyll-a measurements taken by the wirewalkers and seaglider, which were deployed nearby.

Float Number	**Latitude**	**Longitude**	**Time (UTC)**	**Status**
1537	3.00°N	140.00°W	13 Nov 2024 19:30	Working
4001	0.50°N	140.00°W	22 Nov 2024 04:40	Working

Table 5: BGC Argo float deployment summary table

3.6 EM-Apex Floats

Jofia Joseph

Three ElectroMagnetic Autonomous Profiling Explorer (EM-APEX) floats were deployed during this cruise as part of a new observational program, SQUID (Sampling QUantitative Internal-wave Distributions). The program aims to improve the broad-scale characterization of internal wave

climates through global deployments of autonomous profiling floats that measure shear, strain, and turbulent mixing.

The EM-APEX profiling float is a modified Argo-style float designed to provide velocity profiles through the interpretation of electric field measurements. The motion of conductive seawater through the Earth's vertical magnetic field—a process known as motional induction—generates weak electric fields that are linearly related to the horizontal velocity of the water. Due to intricacies of motional induction (see Sanford et al., 1971, or Szuts, 2015), the resulting velocity profile has an unknown offset that corresponds to the electric field from the depth-averaged velocity (plus small scaling adjustments). In addition to velocity measurements, and as per standard Argo requirements, the float is equipped with an onboard CTD (Seabird) for collecting CTD profiles, two sets of FP07 thermistors for turbulence measurements, a GPS unit for collecting surface fixes, and an Iridium modem with an antenna for communicating with a shore server to transmit data and upload new mission commands.

Each float operates by changing its buoyancy to move vertically through the water column. During standard operations, the float descends to a parking depth, remains there for a specified duration, and then ascends while collecting data. At the surface, the float uploads data, downloads commands, and collects GPS fixes. During the ascent, they collect CTD and EM velocity data. The EM-APEX also collects CTD and EM velocity data during descent.

Deployment Details

Float 10332 (Float 1):

- Deployment Location: 4.5°N, 141.73°W
- Rationale: Based on Buijsman et al. (2017), suggesting northbound incoherent internal tide energy flux from the Polynesian Ridge.
- Status: Working

Float 10337 (Float 2):

- Deployment Location: 3.01°N, 140.00°W
- Rationale: Deployed at the northernmost MOTIVE mooring site, an active region of internal wave energy flux as per Buijsman et al. (2017), for comparison with the mooring data.
- Status: Failed due to suspected leakage.

Float 10329 (Float 3):

- Deployment Location: 8.00°N, 140.24°W
- Rationale: Originally planned for deployment at 10°N, 150°W (a weaker internal tide region). After the failure of Float 10337, this float was deployed in alignment with the predictions of the internal tide beam.
- Status: Working

Float Number	Latitude	Longitude	Time (UTC)	Status
10332	4.50°N	141.73°W	12 Nov 2024 00:41	Working
10337	3.01°N	140.00°W	12 Nov 2024 18:49	Failed
10329	8.00°N	140.24°W	02 Dec 2024 17:37	Working

Table 6: EM-APEX float deployment summary table

3.7 Seaglider

Katie Kohlman

A UW Seaglider (SG195) was deployed at 0.73N, 139.16W after the second WireWalker deployment. As the WireWalkers drifted northeast, the glider followed, flying just north of the drifting array. When the WireWalkers drifted southeast, the glider followed a more zonal transect going west to east along 1N (Figure 19) crossing the trailing edge front and observing a salinity front. The glider kept this zonal transect until Nov 28th when it pursued a new course to be sandwiched in between the two Saildrones.

After Nov 28th, the glider then pursued a new course to 1.5N, 140W to perform multiple large scale zonal crossings of tropical instability waves with another coordination with the two Saildrones before flying back to Honolulu, Hi in Feb 2025.

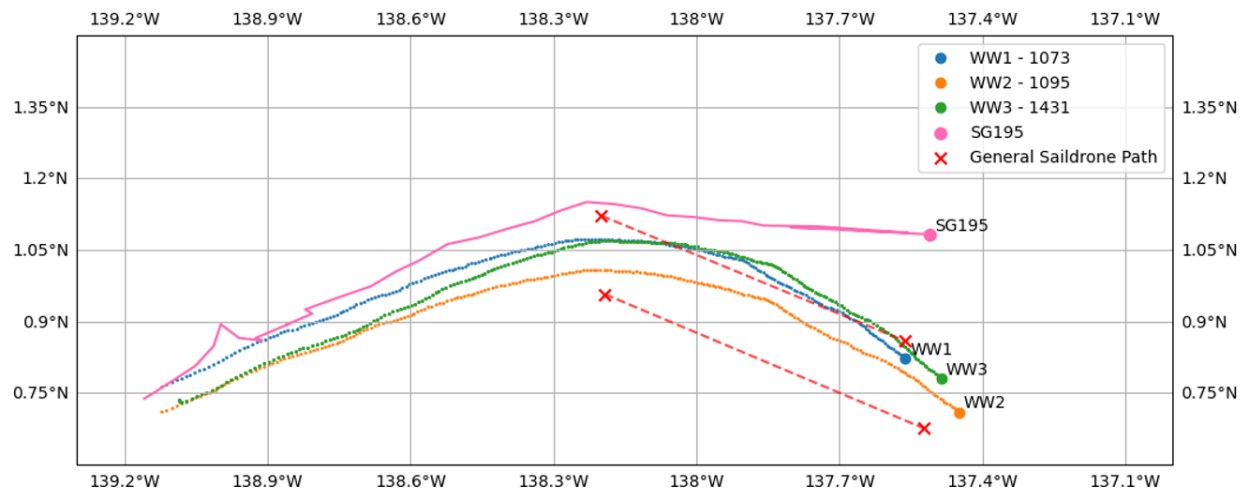

Figure 19: Locations of Seaglider (pink), relative Saildrone tracks (red), and WireWalkers, (orange, blue, and green) as they crossed the front Nov 24-27.

The Seaglider was equipped to measure conductivity, temperature (CT Sail), oxygen (Aanderaa), and fluorescence (700 nm, 695 nm, and 470 nm) (Wetlabs) on both the descents and ascents (Figure 20). It also computes average vertical velocity and depth averaged currents based on modeled vs. observed dives. The glider is currently achieving four 990 m dives a day averaging 20 km a day.

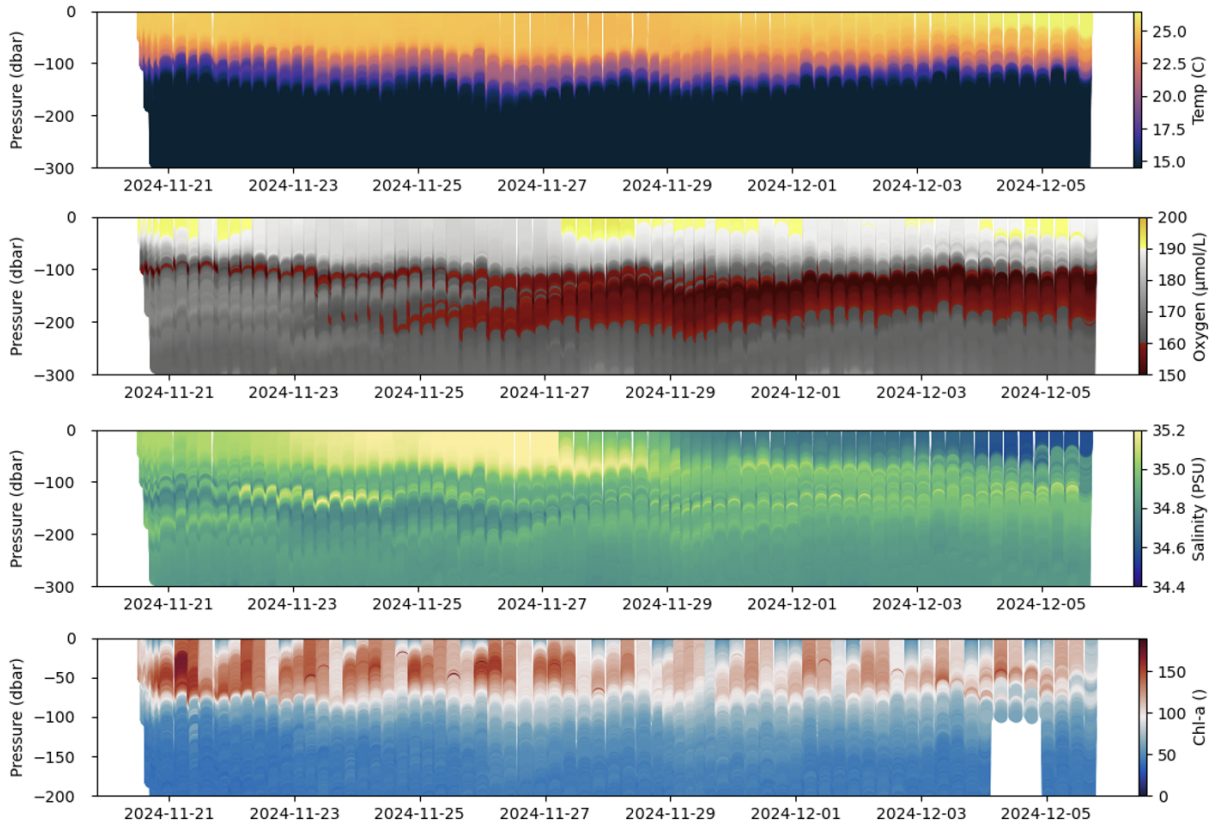

Figure 20: Temperature, Salinity, Oxygen, and 695 nm backscatter observed by SG195 from deployment on Nov 20 to Dec 5 2024.

3.8 Saildrones

Katie Kohlman

As part of the NOAA/PMEL Tropical Pacific Observing System (TPOS) Saildrone Missions, two Saildrones (SD1033 and SD1090) coordinated with various components of the MOTIVE cruise to enhance observational coverage.

Crossing the Front: Beginning on November 24, the Saildrones were positioned on either side of the WireWalker array as it drifted eastward, providing complementary air-sea and upper ocean observations (Figure 19). The positions of the Saildrones were continuously adjusted to stay aligned with the WireWalkers. The tracks of the Saildrones shown in Figure 19 are illustrative; the actual tracks, color-coded by time, are displayed in Figure 21. The R/V Sikuliaq traveled west to east approximately at 1.5° (north of the Seaglider) while conducting fastCTD sampling. Together, the ship, Saildrones, Seaglider, and WireWalkers sampled the same trailing edge of a front. Although the temperature gradient was relatively weak, a significant salinity front was observed.

Triangle w/ Ship: On November 27, 2024, as the R/V Sikuliaq traveled southward to retrieve the WireWalker array, Saildrones 1033 and 1090 positioned themselves to form a triangular array with the ship as the third vertex, surrounding the Seaglider (Figure 22). During this time, the ship's

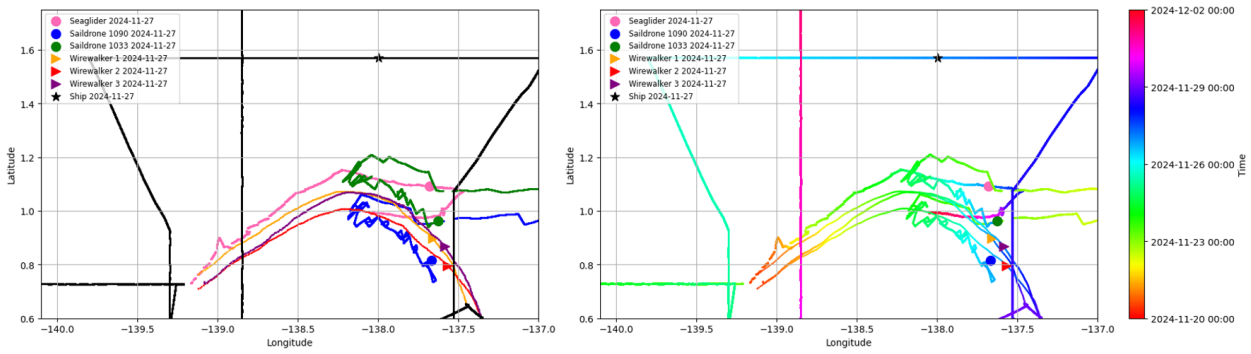

Figure 21: General tracks of R/V Sikuliaq, SD1033, SD1090, SG195, and three WireWalkers on the left. The tracks are color-coded by time on the right figure.

ADCP was operational, and the fastCTD was actively sampling. The distance between SD1033 and the R/V Sikuliaq was 19 km, while the distance to SD1090 was 16 km. The purpose of this triangulation was to enable computations of vertical velocity and vorticity by integrating data from multiple platforms. The R/V Sikuliaq briefly spotted SD1090's blinking lights on the horizon.

Intercomparison at 0N, 140W: By November 29, they departed the region and traveled to 0°N, 140°W to conduct intercomparison studies with the TAO mooring at that location. The Saildrones are scheduled to continue their tropical mission until February 2025. The Saildrones are equipped with instruments to observe a wide range of parameters, including:

- **Surface atmospheric:** wind speed and direction, infrared radiation, longwave radiation air temperature, humidity, barometric pressure, and pCO_2.
- **Surface ocean:** wave height and period, seawater pCO_2, oxygen, temperature (mulitiple thermistors to resolve the top 2 m of the water column), salinity, PAR, and chlorophyll.
- **Subsurface ocean:** currents from 5 m to approximately 100 m depth, measured using an ADCP.

3.9 Using Forecast Models

Anna Deppenmeier

We used the Operational Mercator global ocean analysis and forecast system Glorys at 1/12° horizontal resolution to predict the potential evolution of the TIW front and to estimate WireWalker paths before deployment. The model is based on NEMO3.6 (Madec et al., 2017) and forced by the European Center for Medium-range Weather Forecast (ECMWF) Integrated Forecast System hourly forcing at 1/10th° horizontal resolution. We used the forecast sea surface temperature to obtain insights on the TIW front evolution and forecast velocities with the Lagrangian particle simulator OceanParcels (https://oceanparcels.org/) to simulate the potential WireWalker paths. Ahead of the first deployment we assumed that the WireWalkers would move with the intergated velocities over the entire wire length, 750m. We extracted forecasts of Glorys velocities (available up to ten days out), constructed vertically integrated velocities and performed a number of Lagrangian Particle Tracking experiments to gauge what the likely path of the WireWalkers will be. For the first

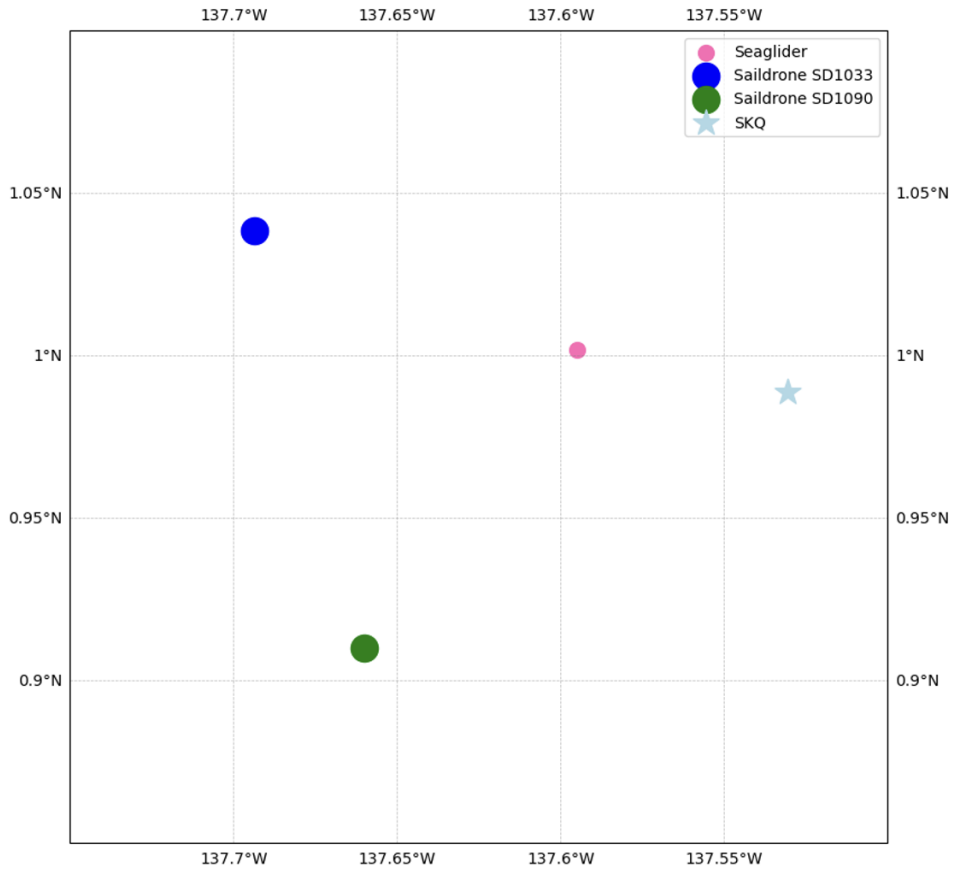

Figure 22: Triangulation made by SD1033, SD1090, and R/V Sikuliaq.

deployment we simulated a number of different TIWs and placements to estimate the spread of the possible paths. Depending on the placement distance from the TIW cold cups front the simulated WireWalkers move north or east-ward, though most of them move westward (Fig. 23). All of the paths except for the northward ones cross the TIW front from warm to cold water of the simulated TIW fronts (not shown). The actual WireWalker path for deployment 1 resembles the northward trajectory, and the TIW cusp passes the WireWalkers on the last day of deployment (Fig. 1). For the second deployment we attempted to simulate the paths with not only the integrated velocities (int in Fig. 23), but also with the surface velocities (sfc) and a combination that weights the surface currents added to the integrated current as 20% (20:80). The surface currents move the WireWalkers very differently from the integrated currents, even though the combination 20:80 proved closest to the observed path in deployment 1 (not shown). In deployment 2 the integrated paths are closest to the observed paths, though we note that the actual WireWalkers move the distance within three days while the forecast takes more than ten days for less of the distance. Comparison of Glorys forecast currents with shipboard ADCP velocities show that while Glorys captures the larger scale patterns of velocity along the ship track reasonably well, Glorys underestimates the strength of the equatorial undercurrent by about 30% (not shown). Discrepancies between forecast velocities and shipboard ADCP and velocities observed by the WireWalkers will be investigated after the cruise.

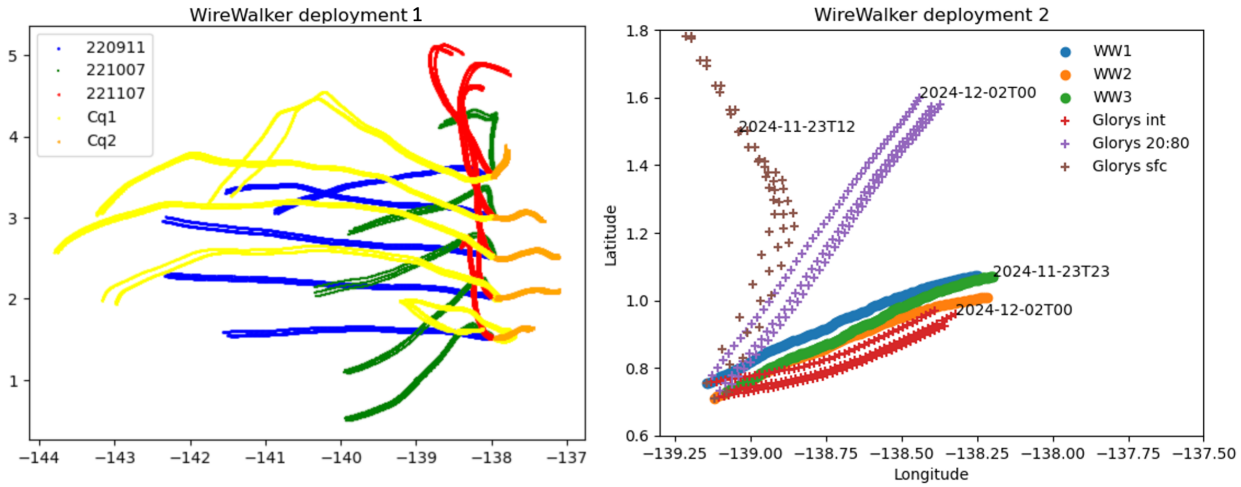

Figure 23: Ocean Parcels simulations with Glorys velocities for WireWalker deployments 1 and 2.

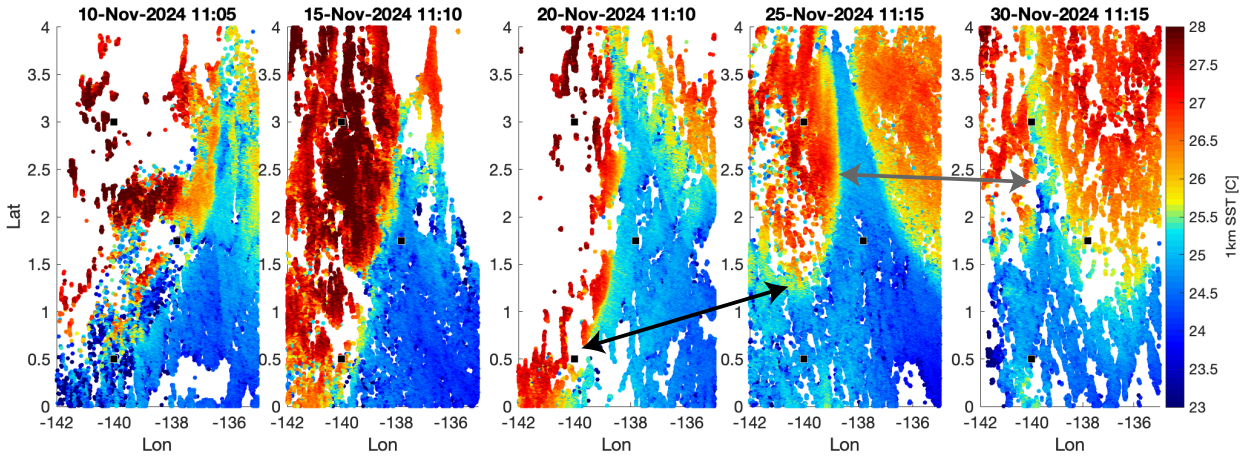

Figure 24: The level 2P sea surface temperature from MODIS during the cruise, spaced 5 days apart showing the TIW front movement. Black squares indicate mooring locations. Note that movement of the TIW is not continuous, the location of the front can be nearly the same between the satellite images, or move dramatically. Two examples of dramatic movement are indicated by the black and gray arrows. White areas are generally clouds. Note that the cloud detection algorithm misses some clouds in the leftmost panel, plotted as cool SSTs.

Scientific Overview

4.1 Tropical Instability Wave Context

Caitlin Whalen

The process studies and larger-scale surveys were conducted in the context of the propagating TIW that moved westward throughout the cruise period. Figure 24 shows high-res MODIS satellite SST in 5-day increments during the cruise period. Generally, the cold TIW cusp begins just west of the mooring array on Nov 10, and by the end of the cruise the tip of the cold cusp is at the northernmost mooring site. Rather than smoothly traveling at the mean TIW propagation velocity of around 43 km/day, the TIW front stalls or travels at much slower speeds during periods of time (e.g. between 0.5-2 N, and Nov 15-20th), and then moves at much faster velocities during other periods (e.g. see black and gray arrows in Figure 24). This variability in propagation velocity suggests that there may be opportunities to generate internal or surface waves during either the transitions between various propagation speeds or during the faster periods.

The internal-wave environment in the thermocline appears to be impacted by the location and possibly the propagation speed of the TIW cusp. Figure 25 shows MODIS SST in the study region from unevenly spaced days over the course of our time there. The black dots indicate the magnitude of the standard deviation of the density between 800-900 m from the FastCTD or EPSI at each location, plotted on the satellite image that was taken closest in time to each occupation with the ship. This suggests that there are large-scale spatial patterns in the isopycnal variability, and hence internal wave activity, that are tided to the placement of the TIW fronts, the latitude, and the frontal movement.

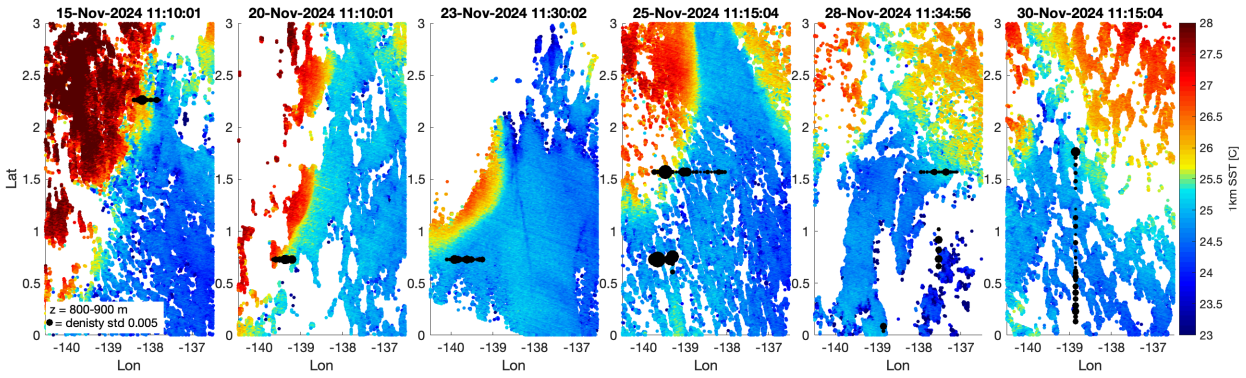

Figure 25: The level 2P sea surface temperature from MODIS during the cruise, note that unlike Figure 24, the satellite images are from unevenly spaced dates, chosen to highlight the various process studies. The black dots indicate the standard deviation of the density between 800-900 m from the Fast CTD or Epsi.

The following summarizes what the observations shown in Figure 25 may indicate. On both Nov 15th and Nov 20th, the standard deviation the density is slightly larger directly underneath the TIW fronts, suggesting elevated internal wave activity associated with the front opposed to either side. On Nov 23th, the front moves away from the area, yet there is little change in the density standard deviation between 800-900 m. However just two days later, on Nov 25th, the standard deviation of the density is elevated at 0.6 N compared to before, consistent with a wave

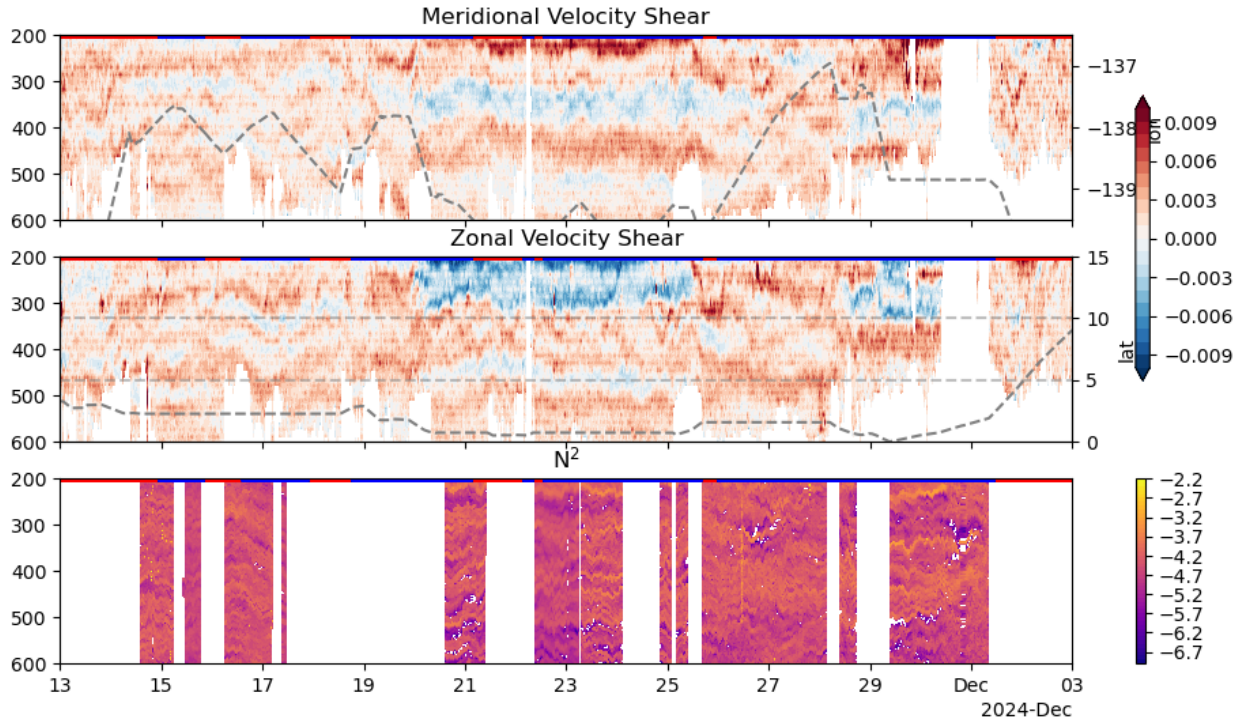

Figure 26: Depth and time section of zonal and meridional shear obtained from the OS75 SADCPs on board and stratification from CTD measurements. The stippled lines in the first and second row show longitude and latitude respectively, the blue and red bars denote times when the sea surface temperature was lower (blue) or higher (red) than 26°C.

that is generated near the surface and then propagate downwards, perturbing the isopyncals at depth. Also on Nov 25, the largescale survey near 1.6 N again suggests that there may be elevated internal wave activity beneath the front opposed to underneath the center of the cold cusp. The front associated with the trailing edge of the cold cusp is generally weaker, and is the associated density standard deviation is low as shown on Nov 28th. Finally, the large-scale N-S section shows larger standard deviations in the density within 0.5 degrees of the equator opposed to further north, with the exception being one bin with a larger standard deviation directly beneath the front at the trailing edge of the cold cusp (Nov 30th). Note, that this analysis is preliminary since the density variance would also be impacted by ship speed and instrument fall rate, which has not been taken into account yet here.

4.2 Shear Layer Cake and Stratification

Anna Deppenmeier

Early on in the cruise we started observing a strongly layered structure of both shear and stratification. To assess the meridional structure of the 'layer cake' we show the meridional and zonal velocity shear as well as the stratification together with the latitude and longitude at the time of the measurements (Fig. 26).

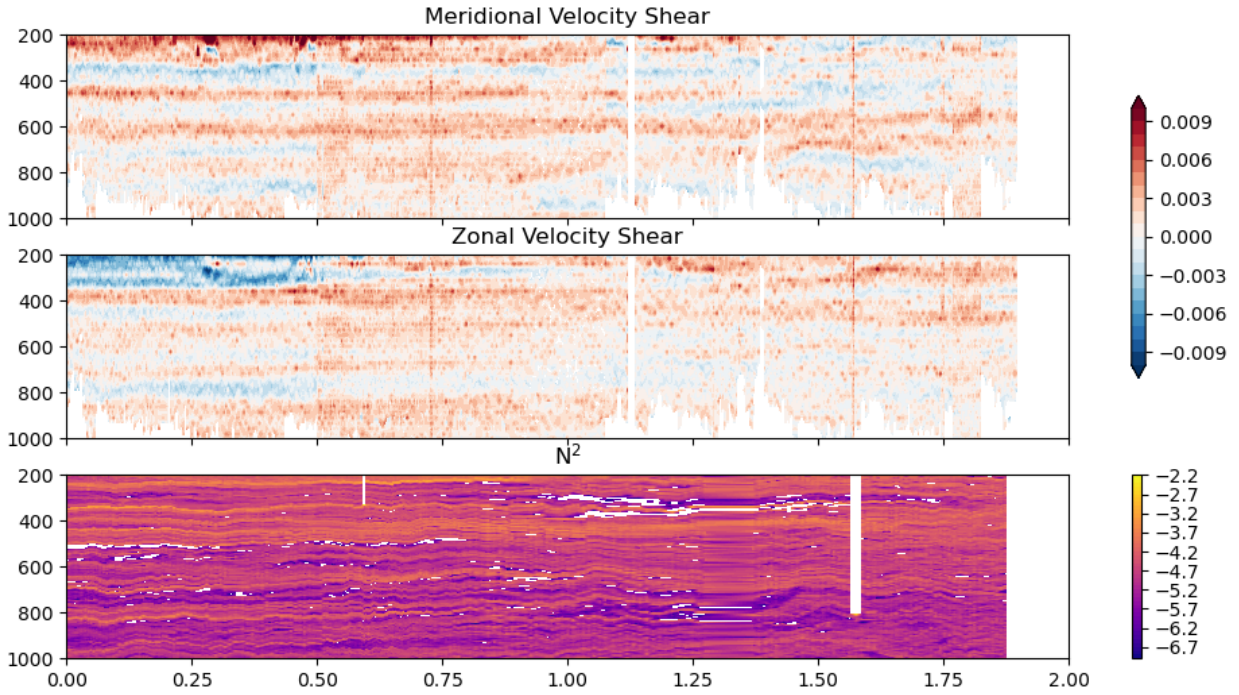

Figure 27: Depth and latitude section of zonal and meridional shear obtained from the OS38 SADCP on board and stratification from CTD measurements along the meridional line starting at the Equator and finishing at around 1.8°N. The stippled lines in first and second row show longitude and latitude respectively, the blue and red bars on the top x-axes denote times when the sea surface temperature was lower (blue) or higher (red) than 26°C.

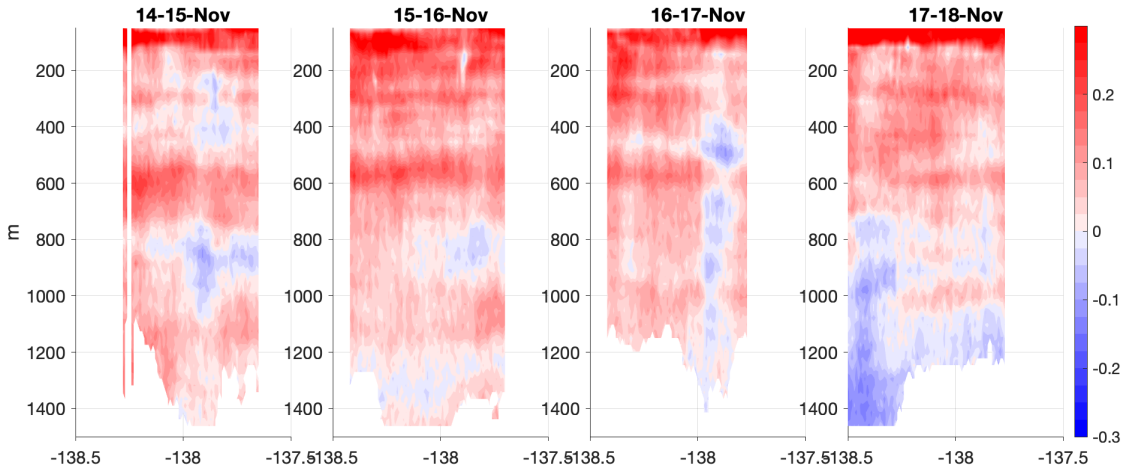

Figure 28: Meridional velocity across the leading edge of the TIW front at 2.3° N. Each subplot is a different transect along the same latitude. Note the upward phase propagation with depth of the bands of meridional velocity, particularly between 800-1400 m.

The layered structure can be seen until at least 5°N, though the stratification structure becomes less strongly pronounced at around 2°N (Fig. 27).

4.3 Yanai and Lee Waves

Waen Anutaliya

Meridional velocity was used to better understand Yanai wave activity in the region. The meridional velocity generally reverses multiple times with depth over all the measured transects (Figure 5, 28, 29, 30). Upward phase propagation of the reversing meridional velocity bands was evident at the 2.3° N zonal transect (section d7 - d10) with a propagation speed of 30 m/day (Figure 28) which resembled a Yanai wave in the Indian Ocean (Smyth et al., 2015). Such northward phase propagation was not clearly observed in the other measured transects. The repeated transect at 0.7° N (section d13 - d16) showed that the vertically reversing band propagated eastward with a speed of 0.2 m/s (Figure 29, 3rd and 5th column). While this band seemed to be larger at 0.7° N (250-300 m vertically) compared to the one at 2.3° N (200 m vertically), the elevated background shear layer cake may also play a role (Figure 28, 29).

Unfortunately, the shipboard ADCP only resolved velocity to approximately 1000 m during the large-scale zonal (section d18) and the two meridional transects (section d19 and d20) with some profiles reaching only to a depth of 750 m (Figure 30). With the presence of the strong shear in the region, the meridional velocity did not provide clear evidence of a Yanai wave.

It is worth noting that a Yanai wave with a vertical wavelength of 600 to 1000 m at the equator has a trapping latitude between 1.0° and 1.3°. The trapping latitude implies that the meridional velocity contributed by a Yanai wave at 2.3° N is only 7-21% of the value at the equator. Therefore, a more careful investigation is needed to be confident that a Yanai wave is present in the study region.

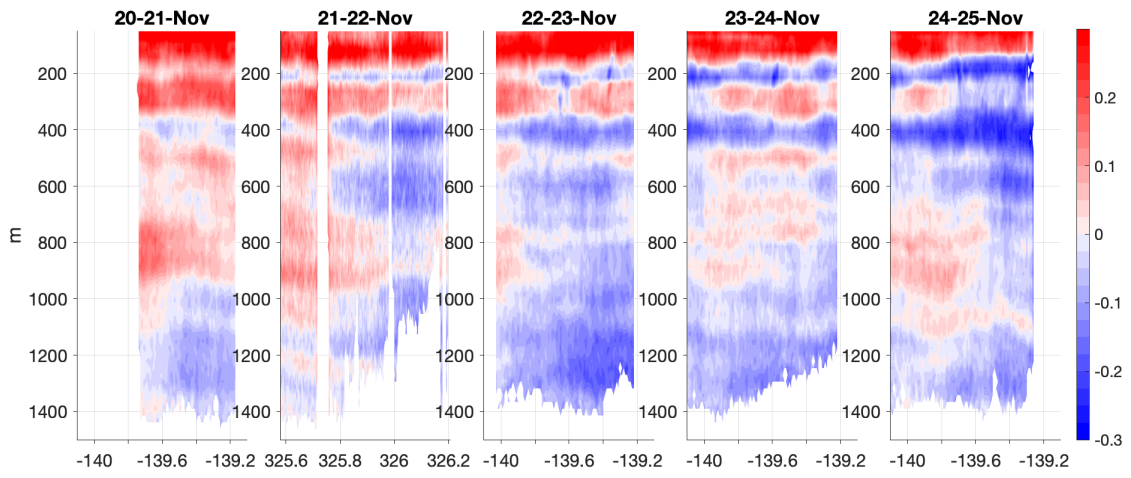

Figure 29: Meridional velocity across the leading edge of the TIW front at 0.7° N (first and third to fifth column) and meridional velocity during Mooring A deployment at 0.5° N, 140° W (second column).

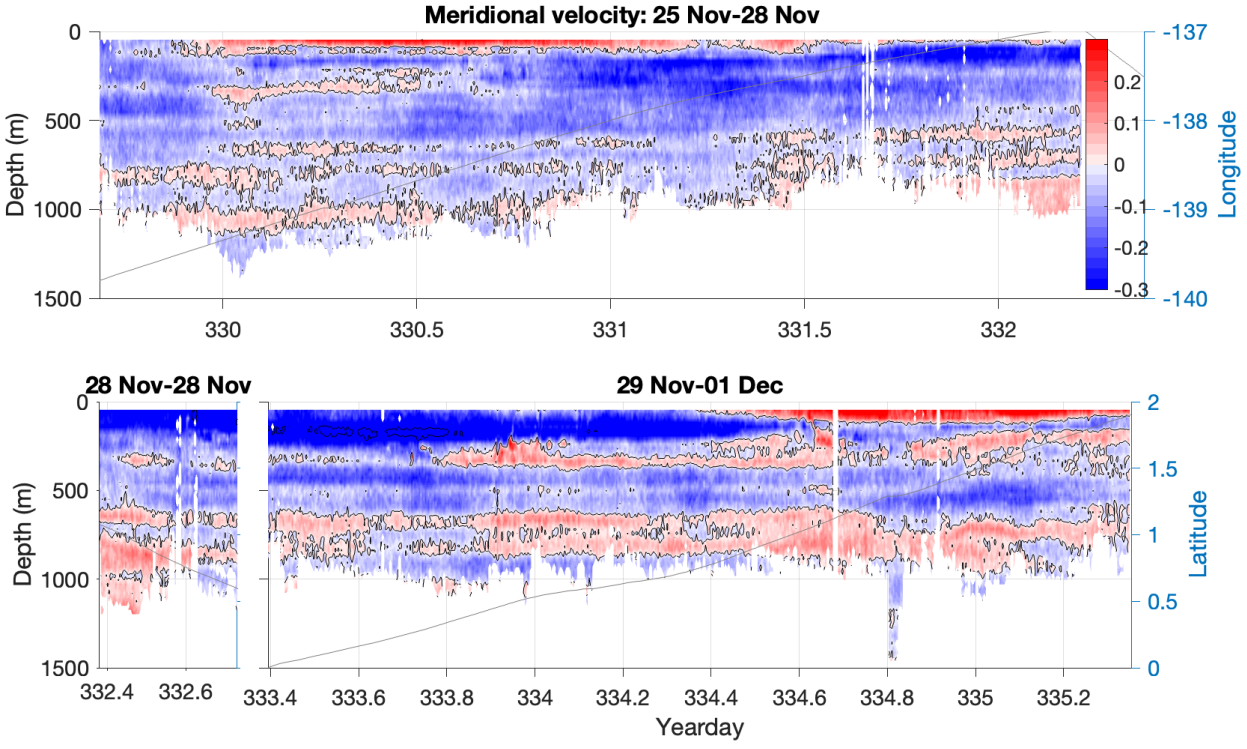

Figure 30: Meridional velocity at the 1.6° N large-scale zonal transect across the TIW (top), at the 137.5° W meridional transect upstream of the wirewalkers (bottom left), and at the 138.9° W large-scale meridional transect (bottom right).

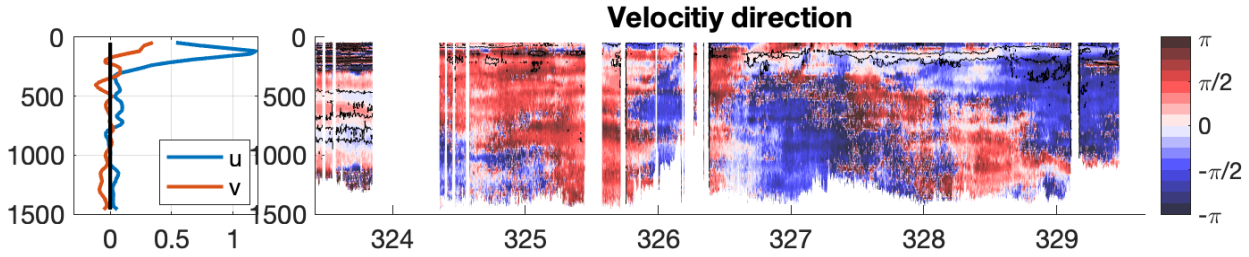

Figure 31: (Left) Mean zonal (blue) and meridional velocity (orange) and (Right) direction of current anomalies along the recurring transect at 0.7° N.

High-frequency variability of isopycnal depth below 500 m as well as high variability in density displacement were observed on the cold side of the leading edge of the TIW front along the recurring 0.7°N transect (e.g. Figure 11). The shipboard ADCP also showed alternating bands of meridional velocity that changed its direction over time which was most clearly seen between 200 and 600 m depth (Figure 29). The direction of the anomalous current was calculated to understand how the velocity changed with time and depth in this region (Figure 31); it revealed a clockwise rotation of the anomalous current in time and upward propagation in the water column from yearday 326.5 to 329. This rotation had a period of 2 days and downward group speed of approximately 800 m/day with a slower propagating speed away from the front (e.g. yearday 328 – 329) which are similar to the characteristics expected from TIW-generated Lee waves. The rotation of the anomalous current was only observed along the 0.7° N transect which might be due to the sharpness and the westward propagation of the TIW front at the time of measurement.

4.4 Lee Waves in a Model

Ellen Davenport

As described above, we were interested in finding observational evidence for the lee waves in Tanaka et al. (2015). In order to identify observable characteristics of these lee waves, we analyzed output from the Tropical Pacific Ocean State Estimate (TPOSE).

TPOSE has $1/6th$ degree horizontal resolution, with 2m vertical resolution in the upper ocean. This model is the product of 4-dimensional variational data assimilation (4DVAR). Assimilated data includes SSH, SST, Argo profiles, and ships of opportunity. The state estimate is forced with hourly reanalysis from ERA5. Validation of TPOSE shows that TIWs in the model are in phase with observations.

TPOSE covers the years 2012-2016. We specifically used model output from October-November 2012, which was an ENSO neutral period and qualitatively compares well to November 2024. Tanaka et al. identify lee waves through their signature in the vertical velocity anomaly. We were able to identify a very similar phenomenon in TPOSE. The progression of a lee wave example from TPOSE is shown in Fig. 32. This particular example wave has a horizontal wavelength of approximately 75km with a period of about 4 days. Given a background EUC velocity of 0.75m/s, this estimated wavelength and period fit the dispersion relation for lee waves. We found that the vertical propagation speed of this wave is approximately 700-800 m/day which agrees with the propagation of the observed phenomenon described in Fig. 31.

Unfortunately, vertical velocities are difficult to observe as they are orders of magnitude smaller

than the horizontal velocities. For example, the vertical velocity anomalies associated with these lee waves are on the order of 10^{-3} or 10^{-4} m/s. In order to identify this phenomenon from observations, we used TPOSE to explore the lee wave signature in density, horizontal velocity, and shear. Fig. 33 shows the same lee wave from Fig. 32 along with zonal shear (middle) and shear squared (bottom). In this example there is a clear bump in isopycnals which looks to be associated with increased zonal and total shear.

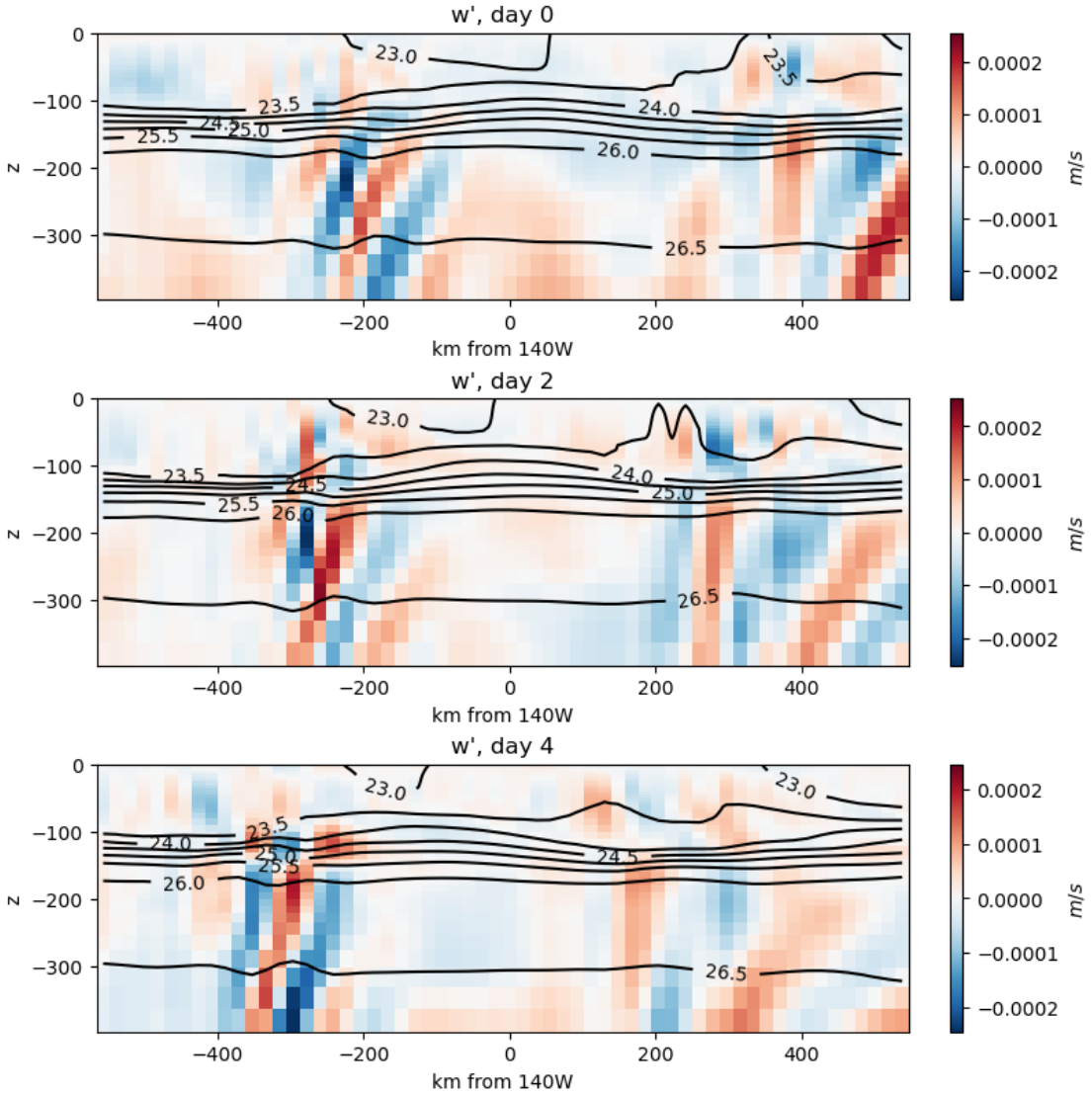

Figure 32: Model output from TPOSE. Longitudinal transect of filtered vertical velocity anomaly at three points in time. The transect is located at 0.75N and is centered at 140W. Each snapshot is 2 days apart. The x-axis shows distance from 140W in km, where West is negative and East is positive. Black contours are density in $kg/m^3 - 1000$. The signature of the lee wave starts near the front and is carried west with the front over time.

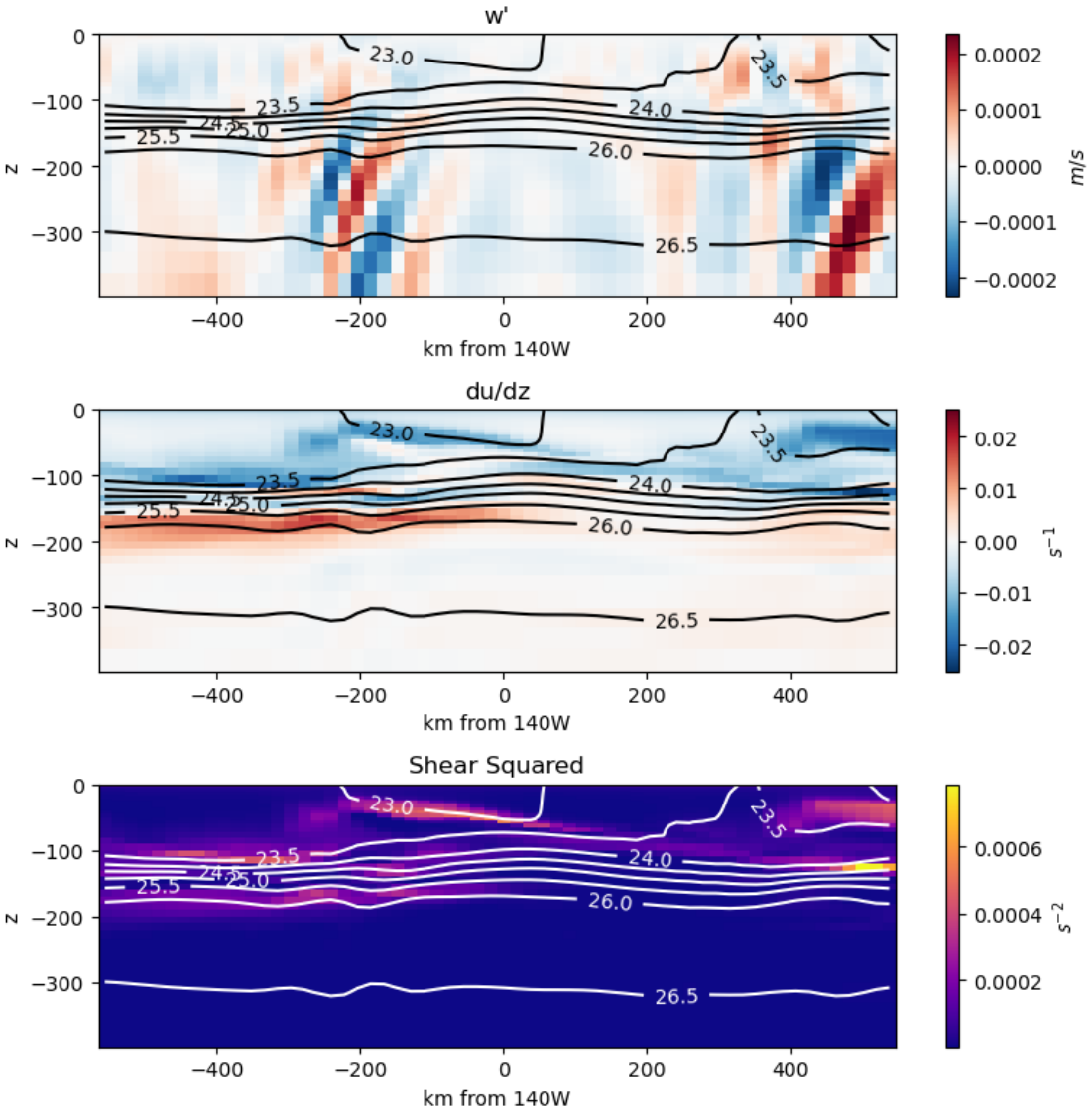

Figure 33: Model output from TPOSE. Filtered vertical velocity anomaly (top), zonal shear (middle), and shear squared (bottom). Observable lee wave signatures include bumps in isopycnals and increased shear. Contours are density in $kg/m^3 - 1000$.

4.5 Fronts

Zoe Caspar-Cohen

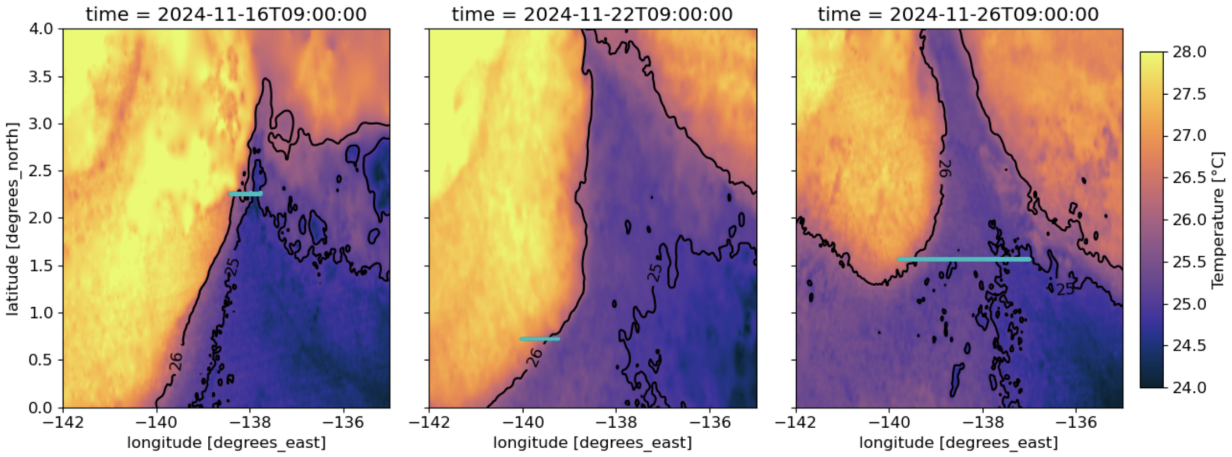

Figure 34: Daily averages of surface temperature from satellite altimetry (NASA/JPL, 2015) during the three sections done during the cruise. Sections are represented by the blue lines.

The sea surface temperature signature of TIWs can be characterized from satellite data as a succession of warm eddies and cold cusps (Figure 34). Each cold cusp, i.e. colder water, is surrounded by two warm eddies, forming two fronts: one west at the leading edge and another east at the trailing edge. During this cruise we were able to cross these fronts several times. Two small transects were realized across the front at the leading edge, around 2.26°N and around 0.73°N (blue lines in Figure 34a and 34b, respectively). Another larger transect crosses both leading and trailing edges around 1.57°N from 139.79°W to 137.00°W (blue line in Figure 34c). Transects provide temperature, T, and salinity, S, down to 750m and 1000m depth depending on the section. Datasets from the ship are also available: T and S at the surface, velocity from ship ADCP. Ship ADCPs provide velocity using different frequencies: 300, 75 and 38 Hz. The higher the frequency the better the vertical resolution is but the data is then limited to a shallower depth range (∼100m for 300Hz to ∼1400m for 38Hz).

In agreement with the data from high resolution (1km) satellite products (NASA/JPL, 2015), the ship underway data shows that 26°C is a good approximation to define the front at the surface. It allows us to follow the cold cusps edge's evolution with time efficiently as the TIW propagates westward (Figure 34). However, the change of water properties between warm eddies to cold cusp varies with time. We observed differences in the temperature, salinity and velocity horizontal gradients between each of the sections at the same latitude. Although the core of warm eddies is warmer than 26°C, the front with the cold cusp shows a temperature that varies from 27 ° C to 25 ° C at the leading edge (Figure 35 black oval). This decrease in T is associated with an increase in salinity and density. The water properties in the cold cusp vary depending on the observation area. In general, the temperature remained below 25.5 ° C, reaching 24.7 ° C. However, at higher latitude, where the cusp is narrow (Figure 34 left), salinity reached its peak around 34.93 and then decreased again down to 34.75 for two of the sections (Figure 35 blue rectangle). Later in the cruise and at lower latitude, the cold cusp water has higher salinity and density, peaking at 35.18 psu and 23.3, respectively (Figure 35 red oval). The data at the trailing edge show a progressive increase in

temperature and a decrease in salinity and density as the front was crossed (Figure 35 green dots).

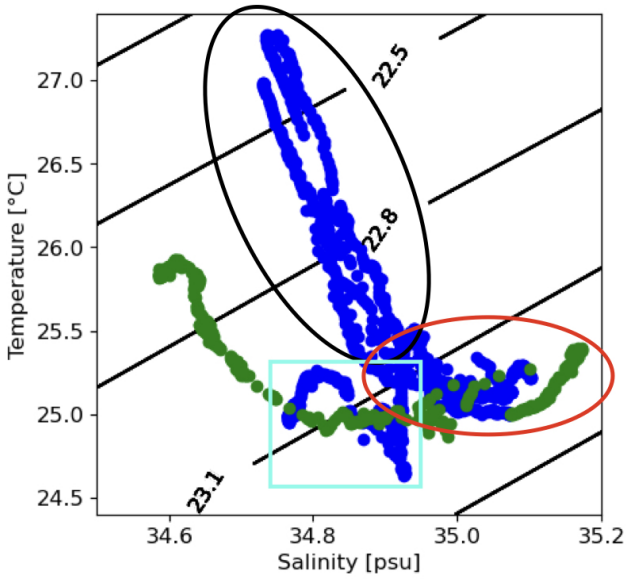

Figure 35: TS diagram from ship underway over zonal sections across the front from Nov.14 to Nov.25. Blue dots correspond to data collected at the leading edge and green dots to data in the trailing edge. Black oval highlight data in the warm eddy, red oval to data in the southern cold cusp and blue rectangle to data in the northern cold cusp.

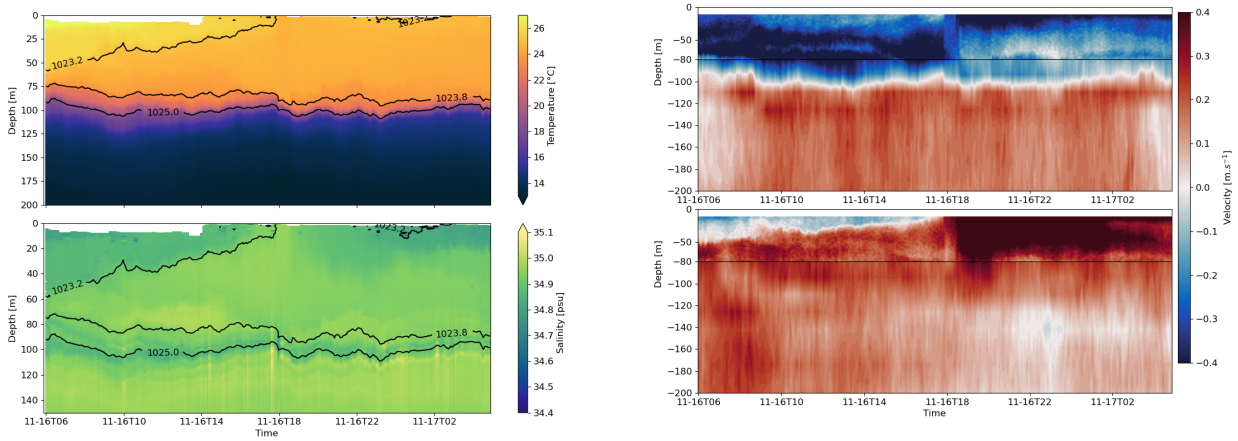

(a) T-S transects from FastCTD.

(b) Velocity field from ship ADCP.

Figure 36: Properties of the TIWs front along a transect, around 2.26°N, between November 16th and November 17th. (a) Temperature (top) and salinity (bottom) sections across the TIWs front. (b) Zonal (top) and meridional (bottom) velocity fields from ship ADCP. Upper 80m are provided using a 300Hz ADCP and lower levels using 75Hz.

The 2D structure of the TIW front remained shallow throughout the observation time period,

limited to the upper 60 m (Figure 36). Particularly strong TS and velocity gradients are observed in two of the northern sections, on November 15th and 16th (Figure 36). Between the warm eddy and the cold cusp, there is a narrow path of dense cold and salty water (24.7 ° C and 34.9 psu). This coincides with a sharp gradient of velocity, only observed in those sections. Zonal velocity remains westward but becomes intensified in the upper 30m in the cold cusp compared a uniform westward current in the upper 100m in the warm eddy (Figure 36b, top). The meridional velocity changes from a southward current to a strong northward current in the upper 50m (Figure 36b, bottom). The water masses with colder and saltier properties seem to correspond to local upwelling at the front. However, looking at the satellite sea surface temperature during those days (Figure 34left), the possibility of advected waters from southeast, i.e equatorial cold tongue, is more likely. These colder, and presumably saltier, waters seems to be advected in the cold cusp by the TIW, mostly staying in the southeastern part. They seem to be brought in the northwestern part if the current is particularly strong, like the ones observed in our sections.

4.6 Deep Cycle Turbulence

Caique Dias Luko

During the second wirewalker deployment, the array placed at about 0.7°N drifted east for about 8.5 days, sampling from the TIW leading edge front to the proximity of the trailing edge front (Figure 2). Along its journey, the wirewalkers experienced an environment of low upper-ocean stratification, and strong shear at the pycnocline (Figures 38 and 37). A recurrent feature observed during the deployment was the formation of a shallow stratified warm layer that starts descending down in the early afternoon (Figure 38). Along with the descent of the warm layer, we observe the descent of a shear layer that reaches the pycnocline (70-100m) every day (Figure 37).

These observations might be associated with off-equatorial deep cycle turbulence. The triggers of deep cycle turbulence are still under debate, and there could be several. One well-supported theory involves the descent of a surface shear layer that reaches a marginally stable region between the mixed layer and the upper edge of the EUC. During the daytime, solar heating causes the surface mixed layer to shallow and stratify. Persistent winds impart momentum to the mixed layer increasing the surface current and the shear near the mixed layer base. As the surface begins to cool in the late afternoon, this shear layer descends, triggering turbulence in the marginally stable layer below. This enhances vertical heat fluxes that cool the mixed layer. Deep cycle turbulence has been widely observed on the Equator, but there are few (if any) off-equatorial observations. Tropical Instability Waves, which are more common during La Niña, have been shown to modulate the zonal vertical shear at the equator. By acting in concert with deep cycle turbulence, TIWs decrease sea surface temperature acting as a positive feedback to ENSO.

Off-equatorial deep cycle turbulence has not been observed yet. However, modeling studies indicate that TIWs can also modulate vertical shear off the Equator. Vortex stretching and titling are responsible for increasing both the zonal and meridional vertical shear inside the TIW cold cusps, making it a suitable environment for the occurrence of deep cycle turbulence. Our measurements indicate that these zonal and meridional descending shear layers do occur and additionally impact chlorophyll and oxygen distributions (Figure 38). The descent of the shear layers erodes the shallow stratified warmer waters, allowing phytoplankton to grow all the way to the surface. Moreover, with the descent of the shear layers, we also observe pulses of oxygenation in the upper 40 m.

These observations were located in the cold cusp and strongly contrast with what was observed on the warm side of the TIW leading edge front during the first wirewalker deployment (Figures 1,

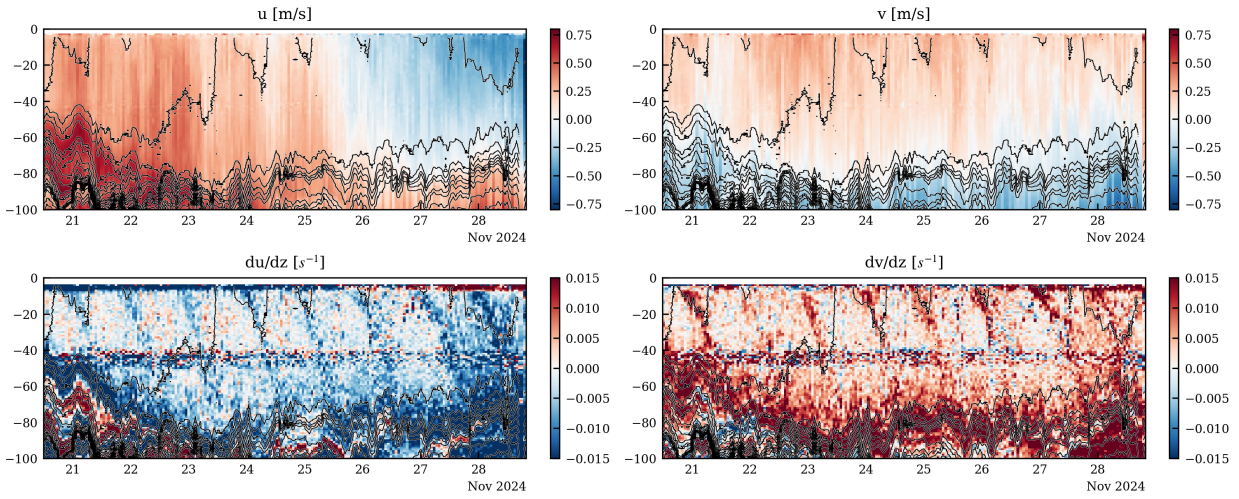

Figure 37: Zonal and Meridional velocities and shear across a TIW cold cusp. Measurements are from the second deployment of WW2. Solid black lines show isopycnals spaced every 0.1 $kg\,m^{-3}$.

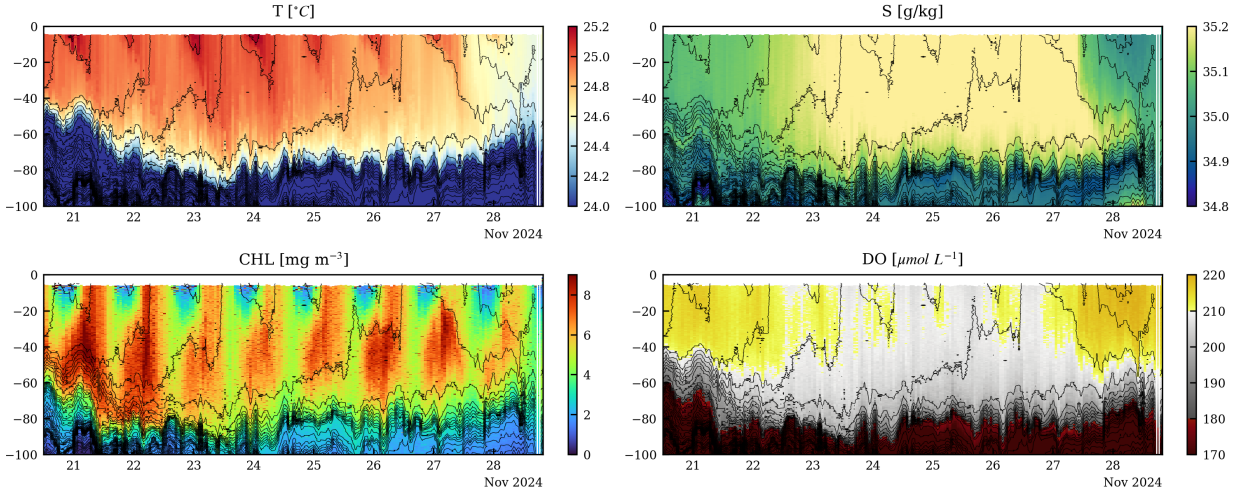

Figure 38: Temperature, Salinity, Chlorophyll and Dissolved Oxygen concentration across a TIW cold cusp. Measurements are from the second deployment of WW2. Solid black lines show isopycnals spaced every 0.1 $kg\,m^{-3}$.

39 and 40). In that scenario, we observed a more stratified upper ocean that restricted the descent of meridional shear layers to about 25 m (Figure 40). In addition, we observe that the levels of chlorophyll are smaller than in the cold tongue, possibly indicating that the absence of mixing due to deep cycle turbulence might restrict phytoplankton growth by limiting the nutrient supply.

This dataset will be further analyzed to contextualize how off-equatorial deep cycle turbulence evolves on different TIW regimes. Our measurements of turbulence properties will allow us to estimate vertical fluxes of heat, momentum and gasses. The BGC ARGO floats deployed next to the wirewalkers will be used to derive a regression between T-S-O_2-Nitrate that can be applied to

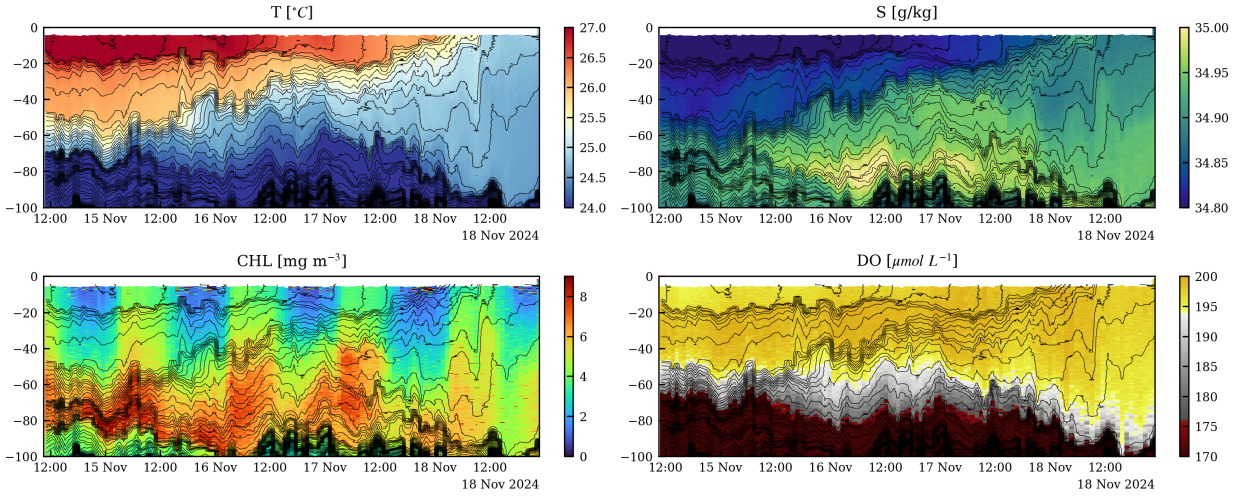

Figure 39: Temperature, Salinity, Chlorophyll and Dissolved Oxygen concentration across a TIW leading edge front. Measurements are from the first deployment of WW1. Solid black lines show isopycnals spaced every 0.1 $kg\,m^{-3}$.

our measurements, allowing estimates of nitrate diffusive fluxes as well. Furthermore, data from the Saildrones and the SeaGlider will also help to contextualize the ocean and atmospheric conditions experienced during the second wirewalker deployment. Finally, the mooring record will allow us to observe how the descending shear layers change in association with TIW and seasonal variability.

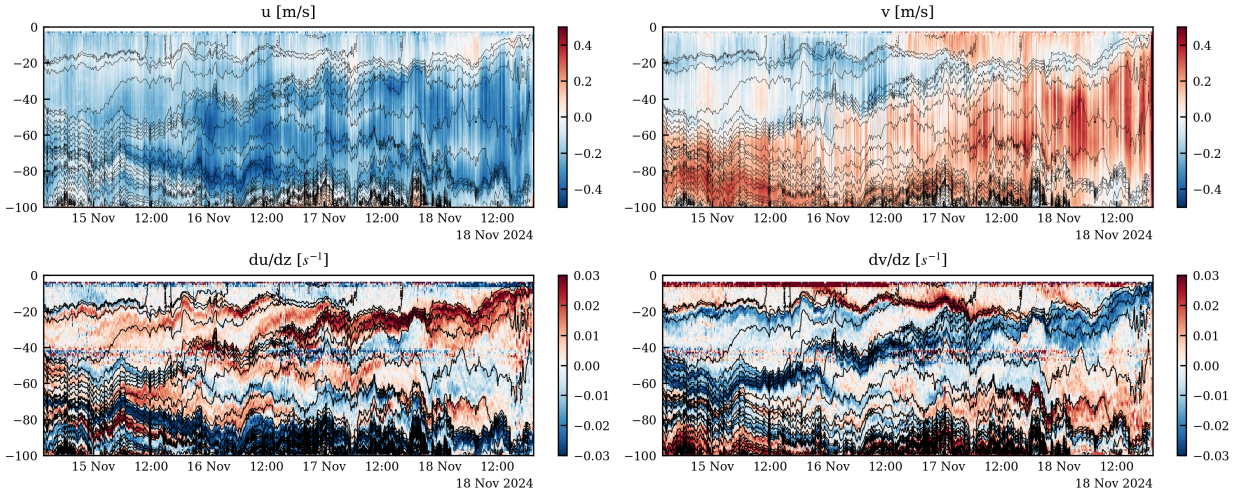

Figure 40: Zonal and Meridional velocities and shear across a TIW leading edge front. Measurements are from the first deployment of WW4. Solid black lines show isopycnals spaced every 0.1 $kg\,m^{-3}$.

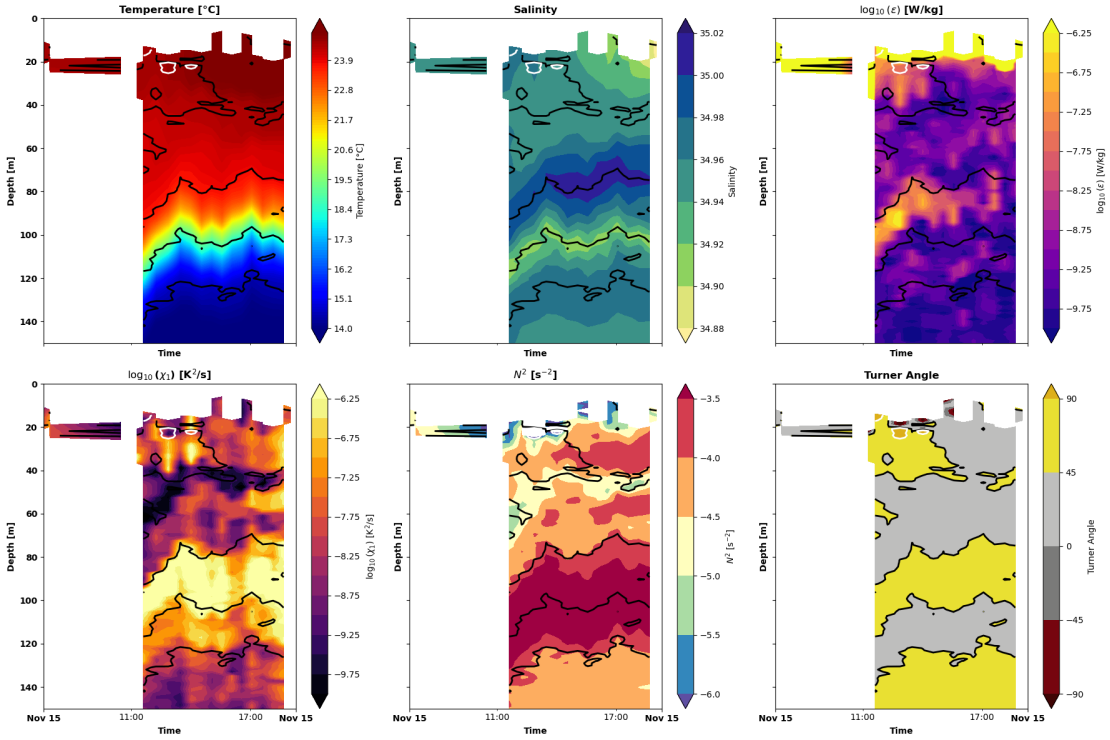

Figure 41: Depth-time section of (a) Temperature, (b) Salinity, (c) $\log_{10}(\epsilon)$, (d) $\log_{10}(\chi)$, (e) $\log_{10}(N^2)$, and (f) Turner angle (degrees) from Epsilometer measurements during the cross-front section, which began at 2.26°N, 137.67°W, on November 15, 2024, at 06:37 (UTC) and concluded at 2.26°N, 138.04°W, at 19:17 (UTC).

4.7 Salt Fingering

Jofia Joseph

In a statically stable water column, where both temperature and salinity increase or decrease with depth, double diffusion occurs because the molecular diffusion of heat is significantly faster than that of salt. The two types of double diffusion in the ocean are salt fingering and diffusive convection. Salt fingering occurs when warm, salty water overlays cooler, fresher water, creating optimal conditions for this process. In contrast, diffusive convection occurs when cooler, fresher water lies above warmer, saltier water within the column.

During the cross-front section that began at 2.26°N, 137.67°W, on November 15, 2024, at 06:37 (UTC) and ended at 2.26 ° N, 138.04 ° W, at 19:17 (UTC), we collected 33 profiles using the Epsilometer. Concurrent measurements of χ and ϵ, along with CTD data, were taken during this transect. A localized subsurface salinity maximum was observed at 80–100 m depth (Figure 41.b). This region was strongly stratified, with a buoyancy frequency on the order of 10^{-3}, sustained primarily by temperature (Figure 41.a). These conditions were conducive to the salt-fingering process, characterized by warm, saline water overlying cooler, fresher water. Turner angle (Tu) values between 45° and 90° further confirmed the presence of salt-fingering conditions (Figure 41.f).

Additionally, we observed enhanced values of χ (Figure 41.d) compared to ϵ (Figure 41.c). These elevated χ values relative to ϵ in double-diffusive processes are attributed to the self-sustained dis-

sipation of temperature variance driven by the intrinsic dynamics of double diffusion, independent of strong turbulent mixing.

References

Madec, G., Bourdallé-Badie, R., Bouttier, P.-A., Bricaud, C., Bruciaferri, D., Calvert, D., Chanut, J., Clementi, E., Coward, A., Delrosso, D., et al. (2017). Nemo ocean engine.

NASA/JPL (2015). GHRSST Level 4 MUR Global Foundation Sea Surface Temperature Analysis (v4.1).

Smyth, W. D., Durland, T. S., and Moum, J. N. (2015). Energy and heat fluxes due to vertically propagating yanai waves observed in the equatorial indian ocean. *Journal of Geophysical Research: Oceans*, 120(1):1–15.

Tanaka, Y., Hibiya, T., and Sasaki, H. (2015). Downward lee wave radiation from tropical instability waves in the central equatorial pacific ocean: A possible energy pathway to turbulent mixing. *Journal of Geophysical Research: Oceans*, 120(11):7137–7149.